J. Mech. Phys. Solids 178 (2023) 105326

Contents lists available at ScienceDirect

Journal of the Mechanics and Physics of Solids

journal homepage: www.elsevier.com/locate/jmps

Crack impinging on a curved weak interface: Penetration or deflection?

M.T. Aranda [a], I.G. García [a], A. Quintanas-Corominas [b,c], J. Reinoso [a,*]

[a] Departamento de Mecánica de Medios Continuos y Teoría de Estructuras, Escuela Técnica Superior de Ingeniería, Universidad de Sevilla. Camino de los Descubrimientos s/n, 41092 Sevilla, Spain

[b] Department of Civil and Environmental Engineering, Imperial College London, London, SW7 2AZ, UK

[c] AMADE, University of Girona, Polytechnic School, c/Universitat de Girona 4, 17003, Girona, Spain

ARTICLE INFO

Keywords:
Curved interface
Crack penetration
Crack deflection
Crack-interface interaction
Finite Fracture Mechanics
Phase field
Cohesive Zone Model

ABSTRACT

Curved weak interfaces present promising advantages to be implemented as crack arrestors in structures designed under the damage tolerant-design principles. Among other advantages, they neither add extra weight nor significantly affect the global stiffness of the structural element, in contrast with alternative crack arrestors concepts. To be employed as a crack arrestor, it is key that the interface is able to deviate the crack. If the crack penetrates across the interface, the effect of the weak interface as a crack arrestor is canceled. In view of this, this work studies how to set the interface parameters to promote crack deviation along the interface. In particular, following the dimensional analysis of the problem, the effect of three significant dimensionless parameters is studied: interface to bulk fracture toughness, interface to bulk tensile strength, and the interface curvature radius normalized with the material characteristic length. The corresponding analysis is carried out using three approaches widely applied for the prediction of cracking events: Linear Elastic Fracture Mechanics, Finite Fracture Mechanics, and a combination of Phase field and Cohesive Zone Model. The results present a clear effect of some parameters, such as the ratio of the interface to bulk fracture toughness, for which the three approaches agree. However, the results are moderately diverse in which correspond to the effect of the ratio of the interface to bulk tensile strength and quite divergent in what respect to the effect of the radius. The results are interpreted and explained as a consequence of the main assumptions behind the approaches studied.

1. Introduction

The demanding interest for the achievement of optimized performance in layered materials and structural systems has stimulated the conception of multiple material arrangements at different scales. These arrangements have been extensively exploited in different applications with a special interest in fracture resistance capabilities. This trend ranges from the conception of multilayered systems at the macroscale to engineering the design of microstructures, mimicking many concepts and designs found in nature. Specifically, several investigations aimed at providing a profound mechanical insight into the underlying cracking mechanisms in bio-inspired interface designs, pinpointing their potential for the next generation of engineering products, see Bermejo (2017) and the references given therein.

* Corresponding author.
E-mail addresses: maranda2@us.es (M.T. Aranda), israelgarcia@us.es (I.G. García), adria.quintanas@bsc.es (A. Quintanas-Corominas), jreinoso@us.es (J. Reinoso).

https://doi.org/10.1016/j.jmps.2023.105326
Received 22 December 2022; Received in revised form 5 May 2023; Accepted 20 May 2023
Available online 29 May 2023

Within this context, one of the most relevant aspects that inherently determines the effective fracture toughness of such systems is characterized by the stability of the composing interfaces in conjunction with their ability to engineering the potential crack paths. Representative applications of these events can be found in thermal and environmental barrier coatings (Wang et al., 2012), delamination events in layered ceramics (Bermejo and Danzer, 2010; Carollo et al., 2018) and laminated composite materials (Turon et al., 2006; Maimí et al., 2011; Zubillaga et al., 2014), among many other applications. The importance of these phenomena can be also found in the designs of crack arrestors in many engineering applications, whereby the presence of interfaces plays a major role.

The comprehensive understanding of potential fracture phenomena in heterogeneous materials has been a research topic that has attracted significant scientific attention over the last decades. The competition propagation vs deflection of a crack impinging on an interface is a particular problem within the context of crack path selection, extensively studied for isotropic media (Barenblatt and Cherepanov, 1961; Erdogan and Sih, 1963; Hussain et al., 1973). For interfaces, the crack path selection is strongly affected by the interface properties and has been investigated by different authors (Cook and Erdogan, 1972; Lin and Mar, 1976; He et al., 1991; Zhang and Suo, 2007; Tullock et al., 1994; Alam et al., 2017; Roy Xu et al., 2003; Sundaram and Tippur, 2016; Zeng and Wei, 2017), with relevant contributions on the matter originally proposed by Cook and Gordon via strength-based analysis (Cook and Gordon, 1964) and posteriorly by Gupta and coworkers at biomaterial interfaces, see e.g. Martínez and Gupta (1994). In this concern, it is worth mentioning the seminal contribution on the matter carried out by He and Hutchinson (1989). These authors conducted a rigorous asymptotic analysis relying on Linear Elastic Fracture Mechanics (LEFM) that led to the derivation of an energy-based criterion for crack deflection comparing the ratio between the interfacial and penetrated fracture toughness with respect to the corresponding energy releases rates. Further studies exploiting LEFM concepts concerned different configurations via the use of He and Hutchinson (HH) criterion, which was experimentally validated in different multi-material systems.

Within the last three decades, this prolific research activity has been revitalized due to the advent of novel predictive methods based on numerical techniques, especially using the Finite Element Method (FEM) owing to its inherent versatility. These computational methods do offer very appealing and powerful aspects that allow the limitations of theoretical approaches to be overcome. In this regard, several authors employed kinematic-enriched methods such as the eXtended-FEM (XFEM) for predicting mixed-mode fracture events in multi-material and multi-layered systems, see Stein et al. (2017) and the references therein given. However, numerical approaches recalling enriched kinematics generally require the adoption of ad-hoc crack propagation and kinking criteria and can present notable operative difficulties for tracking the crack path in very complex geometrical configurations and loading cases. Cohesive zone models (CZMs) can efficiently circumvent such limitations due to the preclusion of any external crack growth criteria, due to their inherent conception. Specifically, recalling the early concepts of Dugdale (1960) and Barenblatt and Cherepanov (1961), Barenblatt (1962), CZMs have been widely used for the analysis of layer-substrate systems and in scenarios concerning channel cracks impinging on the interface between the composing layers. CZMs allow bridging the two traditional views on fracture, i.e. strength- and toughness-based visions via the consideration of the fracture-length scale.

In addition to the previous modeling techniques, in the last decade, the so-called Finite Fracture Mechanics (FFM) and the Phase Field (PF) approach of fracture have emerged as powerful predictive techniques with proven abilities for efficiently characterize crack initiation and propagation in a wide range of applications.

From the perspective of FFM, Leguillon (2002) developed a coupled criterion (CC) for brittle fracture that comply with the concomitant fulfillment of the stress and energy conditions at the material point level, which was posteriorly developed for interface cracks by Mantič (2009). FFM exclusively requires the use of the material strength and fracture toughness as input parameters determining the initiation loading, location and length of the potential crack. Current applications of FFM regarded the prediction of failure in V-notched specimens (Yosibash et al., 2006; Carpinteri et al., 2008; García and Leguillon, 2012), composite materials at different length scales (Carraro and Quaresimin, 2014; García et al., 2016), with multiple extensions such as to nonlinear material behavior (Rosendahl et al., 2019; Leite et al., 2021) and fracture dynamics (Chao-Correas et al., 2022), among many others, see García (2014), Weißgraeber et al. (2016) for reviews. Recently, several authors proposed different numerical schemes for the FE-based implementation of the Coupled Criterion (CC) (Li and Leguillon, 2018), whereas Muñoz-Reja and coauthors developed a Boundary Element Method (BEM)-implementation for the CCFFM for interfaces via the exploitation of the Linear Elastic Interface Model (Muñoz-Reja et al., 2020).

Following an alternative methodology, the PF approach of fracture was originally postulated by Francfort and Marigo (1998), who derived a novel formulation via the regularization of the energetic conception of fracture proposed by Griffith (1921). This variational framework is based on the conception of the Griffith fracture as an energy minimization problem, whereby a direct competition between the elastic and dissipated-energy contributions is devised. In this framework, sharp cracks are regularized using a scalar spatially-smooth variable, denominated as the crack-like phase field variable, introducing a critical strength that is related to the regularization parameter ℓ, which can be interpreted as the characteristic internal length of the material. In this regard, as was thoroughly investigated in Tanné et al. (2018), Kumar et al. (2020), Nguyen et al. (2016a), this attribute allows retrieving well-known size effects at small and large length scales. PF methods have become progressively popular due to their ability to simulate intricate fracture events (Bourdin et al., 2000; Wu and Nguyen, 2018), and accommodating different behaviors ranging from anisotropic solids (Teichtmeister et al., 2017), elastoplastic materials (Ambati et al., 2015; Borden et al., 2016), among many others. Alternative applications have also concerned multi-field applications, composite materials, and rock-fracture, to quote a few of them, and other authors have intensively explored the use of alternative solution procedures for the corresponding multi-field variational formalism (Miehe et al., 2015). Within the context of heterogeneous media, Paggi and Reinoso consistently coupled PF and CZM for triggering fracture phenomena for heterogeneous media (Carollo et al., 2017; Paggi and Reinoso, 2017) encompassing a coupling between bulk and interface damage, whereas (Zambrano et al., 2022) proposed a different

numerical strategy based on the combination of PF and CZ-interface methods uncoupling the damage between them. This latter numerical approach provided excellent agreement with respect to theoretical results from LEFM and the alternative study conducted in Parmigiani and Thouless (2006). In addition to the previous techniques, Nguyen et al. (2016b) and Hansen-Dörr et al. (2020) presented alternative formulations in order to account for the effects of the presence of interfaces within the context of the variational approach of fracture.

However, as recalled above, many systems are characterized by the presence of interfaces with non-planar profiles, including textured definitions or wavy patterns which can be accordingly engineered in order to achieve outstanding fracture response. Despite this potential, at present, the vast majority of previous studies have been concerned with scenarios in which a crack with an arbitrary orientation impinges on flat (straight) interfaces. Notwithstanding, structured- and wavy interfaces might lead to crack trapping or retardant phenomena, whose efficiency strongly depend upon the geometric definition in conjunction with the materials (in terms of stiffness, strength, and fracture toughness) characteristics of the interface and the adjoining bodies. Stemming from the scarcity of previous studies on the matter, in this investigation, the problem of the competition between penetration and deflection of a crack impinging at a curved interface is analyzed. The motivation of this work is twofold:

- First, from the point of view of the application of curved weak interfaces as crack arrestors, the objective is to evaluate the effect of the interface radius on the ability of the interface to deviate the crack. Some preliminary experimental evidences by Aranda et al. (2020) showed that the interface radius could take a notable effect on that. These preliminary results are summarized in Fig. 1, where it can be appreciated that smaller radii seem to promote penetration. This could be very positive if confirmed because the curvature radius can be a parameter easy to be tailored. Given these results, it could argue that the straight interface is the optimum because larger radii promote deflection. However, once the crack is deflected, the concave interface showed a better ability to arrest the crack progression through the interface, see Aranda et al. (2020). Thus, for the overall arrestor mechanism, the straight interface could not be optimum. It will be necessary to know the conditions for deflecting of concave interfaces.
- The second objective is to examine the ability of the different approaches studied, LEFM, FFM and PF+CZM, to predict the influence of the main parameters on the competition between deflection and penetration. In addition, since they are three approaches used for the study of similar problems, the comparison for this problem will allow to contribute to the knowledge of the potential relationship between them, in line with previous works, see e.g. García et al. (2014), Cornetti et al. (2019), Molnár et al. (2020). In particular, the effect of a local geometrical parameter such as the curvature radius and its interaction with the material characteristic length is key to understanding how the different criteria deal with this competition for quasi-brittle scenarios. Previous works deal with the effect of other geometrical parameters, such as the distance from the crack tip to the interface (Zambrano et al., 2022). However, to the best of the authors' knowledge, no previous work deals with the effect of the interface local radius.

The document is organized as follows. The problem under investigation is described in Section 2, including a dimensional analysis of it. The Sections 3–5 present the models based on the LEFM, FFM, and PF+CZM approaches, respectively. Finally, the results are compared and discussed in Section 6.

2. Problem description and dimensional analysis

The problem under study concerns the investigation of the competition between penetration and deflection in a crack impinging on a curved weak interface, and the analysis of how the mechanical and geometric properties of the specimen affect the competition between the two main failure mechanisms: (i) crack deflection along the prescribed interface and (ii) crack propagation into the adjacent body. This analysis is designed in such a way that the corresponding results can be taken as reference solutions in order to exploit curved weak interfaces as potential crack arrestors in engineering structures.

The geometry is composed of a relatively large plate containing a straight and horizontal primary crack impinging on a curved weak interface, see Fig. 2. The local curvature radius of the interface at the impinging point is denoted as R. The remaining geometric parameters of the specimen are denoted as in-plane width W, length L, and out-of-plane thickness B. These parameters are related to the radius R using the next ratio: $W = 2R$, $L = 10R$, and $B = 0.1R$. The initial crack is defined from the leftmost boundary of the specimen till the prescribed interface, which is placed at the middle of the specimen width, i.e. the initial crack length is $a_0 = W/2$. The interface is assumed to comply with a very thin adhesive layer t ($t \ll R$), with elastic properties very similar to the material of the bulk in line with the previous experiments from the authors (Aranda et al., 2022). Correspondingly, the adhesive layer is not expected to have any remarkable influence on the overall stress and strain solution of the system prior to the occurrence of either crack deflection or penetration. This assumption, along with the fact that the two materials joined by the curved interface are coincident with each other, enables studying the problem as a homogeneous solid, from the point of view of the elastic analysis. This fact allows focusing on the properties to be designed in the definition of a crack arrestor in a homogeneous structural element: the curvature radius and the contrast on the fracture and strength properties of bulk and interface.

The specimen is subjected to a remote vertical stress σ. This remote stress is increased quasi-statically from zero to a critical value $\sigma^{\max}$, for which the crack either penetrates ($\sigma^{\max}_{\text{pen}}$) or deflects ($\sigma^{\max}_{\text{def}}$) along the interface. The comparison between $\sigma^{\max}_{\text{pen}}$ and $\sigma^{\max}_{\text{def}}$ provides the preferential of the system.

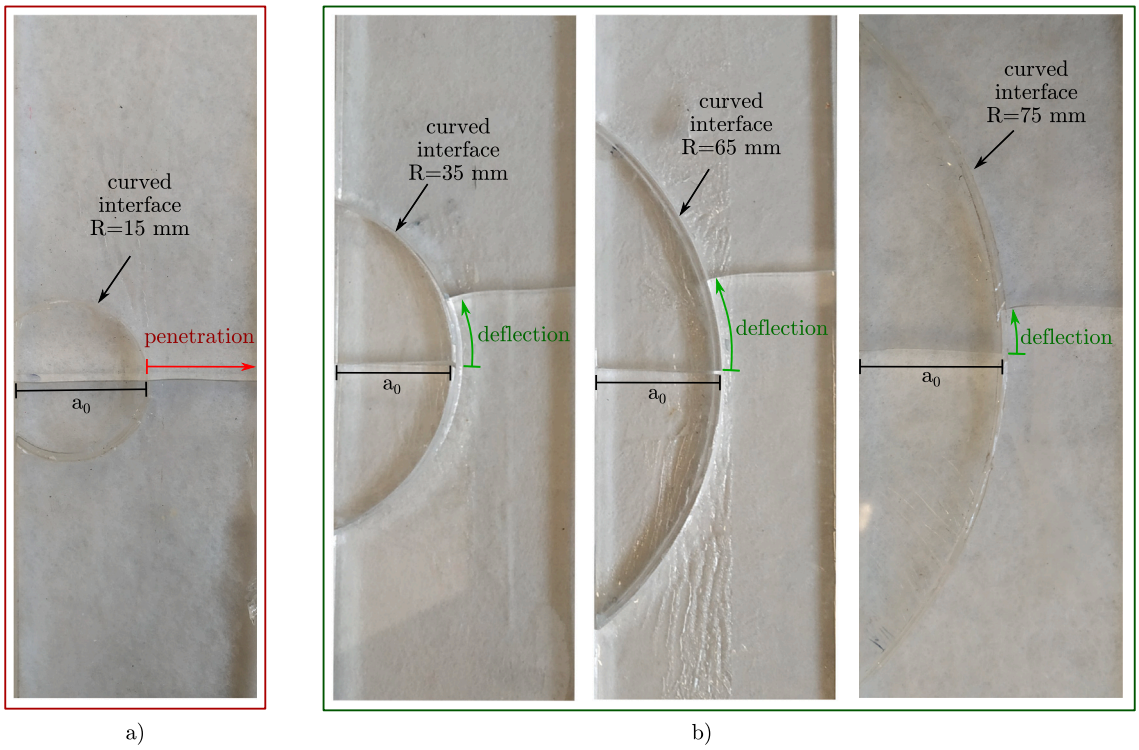

Fig. 1. Photographs of fractured specimens for different radii of curvature of curved interface configuration, showing (a) deflection of the crack path and (b) penetration.

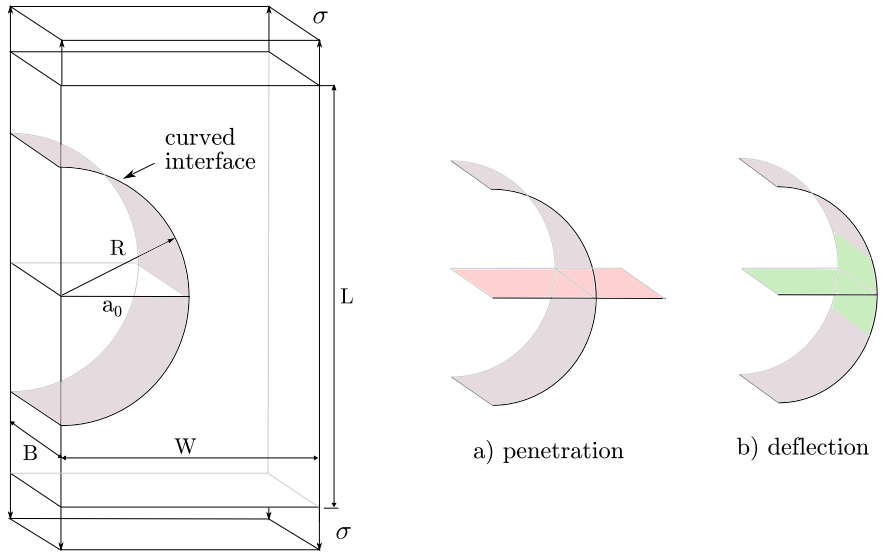

Fig. 2. Schematic of the problem under study: A straight crack implying a curved weak interface.

By conducting the corresponding dimensional analysis of the system, it is possible to identify the main dimensionless parameters governing the problem. In general, the critical stress value ($\sigma_{\text{pen}}^{\max}$ or $\sigma_{\text{def}}^{\max}$) for which the crack either penetrates or deflects can be expressed respectively as the next two functions:

$$\sigma_{\text{pen}}^{\max} = F_{\text{pen}}\left(\sigma_{\text{c}}^{\text{b}}, G_{\text{c}}^{\text{b}}, E, \nu, a_0, W, L, B\right) \tag{1}$$

$$\sigma_{\text{def}}^{\max} = F_{\text{def}}\left(\sigma_{\text{c}}^{\text{i}}, \tau_{\text{c}}^{\text{i}}, G_{1\text{c}}^{\text{i}}, G_{2\text{c}}^{\text{i}}, E, \nu, a_0, R, W, L, B\right) \tag{2}$$

where σ_c^b is the tensile strength of the bulk, and G_c^b is its fracture toughness. The terms σ_c^i and τ_c^i are respectively the tensile and shear strength of the interface. The terms G_{1c}^i and G_{2c}^i are the interface fracture toughness properties for pure Modes 1 and 2, respectively. Finally, the mechanical properties E and ν stand for the Elastic modulus and Poisson's ratio of the bulk.

Based on the previous expression and taking σ_c^b and R as the base set of dimensional units, the ratio between the two previous functions can be rewritten as:

$$\frac{\sigma_{pen}^{max}}{\sigma_{def}^{max}} = \Phi_{comp}\left(\frac{\sigma_c^i}{\sigma_c^b}, \frac{\tau_c^i}{\sigma_c^i}, \frac{EG_c^b}{(\sigma_c^b)^2 R}, \frac{G_{1c}^i}{G_c^b}, \frac{G_{2c}^i}{G_{1c}^i}, \frac{E}{\sigma_c^b}, \nu, \frac{a_0}{R}, \frac{W}{R}, \frac{L}{R}, \frac{B}{R}\right) \tag{3}$$

after the subsequent invocation of the Π-theorem of dimensional analysis. Assuming that the competition between crack penetration and deflection will be ruled by the failure mechanism requiring a lower stress value, the competition can be analyzed through the computation of the former ratio.

It is worth noting that in line with the general description of the problem and the applications, the only geometrical parameter with a relevant role in the current analysis is the interface curvature radius. Thus, in order to avoid any influence of the external geometry on the results, the ratio between the curvature radius and the other geometrical parameters has been fixed. This fact leads to the simplification of Eq. (3) since the geometrical ratios can be removed from the primary arguments. This also holds for scenarios in which these ratios are fixed. Moreover, we assume that the terms E/σ_c^b and ν are fixed since depend upon the mechanical properties of the bulk. Based on this discussion, Eq. (3) can be reduced to:

$$\frac{\sigma_{pen}^{max}}{\sigma_{def}^{max}} = \Phi_{comp}\left(\frac{\sigma_c^i}{\sigma_c^b}, \frac{\tau_c^i}{\sigma_c^i}, \frac{R}{EG_c^b/(\sigma_c^b)^2}, \frac{G_{1c}^i}{G_c^b}, \frac{G_{2c}^i}{G_{1c}^i}\right). \tag{4}$$

The value of this ratio can be associated directly with the possible preferential failure mechanism: (i) penetration in the case of $\sigma_{pen}^{max}/\sigma_{def}^{max} < 1$, and (ii) deflection for $\sigma_{pen}^{max}/\sigma_{def}^{max} > 1$.

Note that in Eq. (4) and based on the characteristics of the present investigation, the dimensionless parameter depending on the radius has been reversed with respect to Eq. (3) in order to provide a direct measure of the dimensionless radius of the interface. Moreover, it is worth mentioning that this parameter can be also rewritten and interpreted as a dimensionless brittleness number, see Carpinteri (1982), Bažant and Kasemi (1990), Mantič (2009) for further details.

It is worth noting that other dimensionless groups could have been chosen. The choice proposed in this work was based on recovering the physical contrasts playing a role in the penetration/deflection competition: on one side the contrast between interface and bulk in terms of fracture and strength properties, and on another side the contrast between the curvature radius and the material characteristic length in the bulk.

Taking as the final form of the Φ_{comp} the expression given in Eq. (4), subsequent contents of the present manuscript will analyze the prospective crack propagation scenarios based on the values of this function using the following well-established failure predicting methodologies: (i) Linear Elastic Fracture Mechanics (LEFM) through the adoption of the classical energy-based Griffith's criterion, (ii) the Finite Fracture Mechanics (FFM) via the use the Coupled Criterion and (iii) Phase Field approach combined with Cohesive Zone Model using nonlinear implicit FE simulations.

3. Linear Elastic Fracture Mechanics

This section presents the prediction of Linear Elastic Fracture Mechanics (LEFM) on the competition between penetration across the interface or deflection along the curved interface. The application of LEFM to this problem will be briefly described, obtaining the expressions governing the competition.

3.1. Model description

According to the energy-based fracture criterion proposed by Griffith (1921), a predefined crack grows when the energy release rate G equals or exceeds the fracture energy G_c. This crack growth can be stable ($G'(a_0) \leq G_c'$) or unstable ($G'(a_0) > G_c'$). In the context of this problem, these conditions are evaluated for the two options herewith considered. The comparison of the critical load for which the conditions are fulfilled in each option will determine the preferential scenario. Note that this is equivalent to the classical He and Hutchinson (1989) approach.

Accordingly, for penetration cases, Griffith's criterion can be expressed as

$$G^{pen} \geq G_c^b \tag{5}$$

where the fracture energy has been identified with the fracture toughness of the bulk material G_c^b in Mode 1, since the crack, in case of penetration, is assumed to grow straight, see Fig. 2.

The energy release rate G^{pen} for penetration can be approximated using the (Takeda and Ogihara, 1994) expression for a free-edge crack in a finite-width plate subjected remote tensile loading σ:

$$G(a) = \frac{\sigma^2 \pi a}{E} F^2\left(\frac{a}{W}\right) \tag{6}$$

where the function F is an explicit function on a/W, see Tada et al. (2000).

Introducing Eq. (6) into Eq. (5), after some manipulations and taking into account that $G'(a) > 0$, the remote load σ for which the crack penetrates $\sigma = \sigma_{\text{pen}}^{\max}$ is given by the following closed-form expression, which has been manipulated in order be expressed as a function of the dimensionless parameters given in Eq. (4):

$$\frac{\sigma_{\text{pen}}^{\max}}{\sigma_{\text{c}}^{\text{b}}} \geq \underbrace{\frac{1}{\sigma_{\text{c}}^{\text{b}}}\sqrt{\frac{G_{\text{c}}^{\text{b}} E}{R}}}_{\gamma} \sqrt{\frac{1}{\pi \frac{a_0}{R} F^2(a_0/(2R))}} \tag{7}$$

where the dimensionless brittleness number $\gamma = (1/\sigma_{\text{c}}^{\text{b}})\sqrt{G_{\text{c}}^{\text{b}} E/R}$ proposed by Mantič (2009) can be identified, or equivalently the inverse of the square root of dimensionless radius $R/(EG_{\text{c}}^{\text{b}}/(\sigma_{\text{c}}^{\text{b}})^2)$ (that can be interpreted as the ratio between R and a number proportional to the well-known Irwin length l_{Irwin} within LEFM context). Finally, the previous expression renders:

$$\frac{\sigma_{\text{pen}}^{\max}}{\sigma_{\text{c}}^{\text{b}}} \geq \frac{1}{\sigma_{\text{c}}^{\text{b}}}\sqrt{\frac{G_{\text{c}}^{\text{b}} E}{R}} \sqrt{\frac{1}{\pi F^2}} \tag{8}$$

with F^2 corresponding to the value of this function for $a_0/(2R) = 0.5$, since $a_0 = W/2 = R$ as discussed in Section 2. Since this argument remains constant in this investigation, the argument of the function F will be omitted in subsequent developments.

Following a similar procedure, for deflection scenarios, the cracking propagation condition is given by

$$G^{\text{def}} \geq G_{\text{c}}^{\text{i}} \tag{9}$$

where G^{def} is approximated using the expression by Leblond (1989) for an abrupt deviation of a crack from a primary crack. Exploiting this approach, the energy release rate for deflection corresponds to the energy release rate of the primary crack multiplied by a particular factor:

$$G^{\text{def}} = \frac{\sigma^2 \pi a}{E} F^2\left(\frac{a}{2R}\right)\left(Q_{11}^2(m) + Q_{21}^2(m)\right) \tag{10}$$

where F replicates the same function previously employed for penetration cases, and $Q_{11}(m)$ and $Q_{21}(m)$ are functions that exclusively depend on the deviation angle, see Leblond (1989), Amestoy and Leblond (1992). In this case, the deviation angle is $\pi/2$ since the crack impinging perpendicularly on the interface, and therefore the particular values of Q_{11} and Q_{22} are set constants for the purposes of this work. It is worth mentioning that in the present analysis, the value of this angle is independent of R because the very first crack growth is considered as an infinitesimal propagation.

With respect to the right-hand side of Eq. (9), the fracture energy, in this case, is affected by the fracture-mode mixity. The dependence of fracture energy upon the fracture-mode mixity has been extensively investigated by different authors, see e.g. Hutchinson and Suo (1992), Banks-Sills et al. (2000). The case of a crack growing along a thin interface, with similar elastic properties to those of the bulk, was recently studied by the authors (Aranda et al., 2022), pinpointing that the phenomenological law by Hutchinson and Suo (1992) can be taken as an accurate approximation for this case. The particular form of the fracture criterion proposed in Hutchinson and Suo (1992) renders

$$G_{\text{c}}^{\text{i}} = G_{1\text{c}}^{\text{i}}\left(1 + \tan^2(1 - \lambda(G_{2\text{c}}^{\text{i}}/G_{1\text{c}}^{\text{i}})\psi)\right) \tag{11}$$

where λ can be expressed as a function of the ratio $G_{2\text{c}}^{\text{i}}/G_{1\text{c}}^{\text{i}}$:

$$\lambda = 1 - \frac{2}{\pi}\arctan\left(\sqrt{\frac{G_{2\text{c}}^{\text{i}}}{G_{1\text{c}}^{\text{i}}} - 1}\right) \tag{12}$$

and ψ is the stress fracture mode-mixity, which can be expressed as a function of Q_{21} and Q_{11}:

$$\psi = \arctan\frac{Q_{21}}{Q_{11}}. \tag{13}$$

Moreover, in line with the previous discussion, Q_{21} and Q_{11} can be considered as constant values for the particular problem under consideration. This yields that the mixity angle ψ can be also taken as constant.

Further steps in the current procedure encompass the insertion of Eqs. (10) and (11) into the original balance Eq. (9). Thus, after some algebraic manipulations and taking into account that $G^{\text{def}\prime}(a) \geq 0$, the remote load $\sigma = \sigma_{\text{def}}^{\max}$ for which deflection scenario is expected, renders:

$$\sigma_{\text{def}}^{\max} \geq \sqrt{\frac{G_{1\text{c}}^{\text{i}} E\left(1 + \tan^2(1 - \lambda(G_{2\text{c}}^{\text{i}}/G_{1\text{c}}^{\text{i}})\psi)\right)}{\pi a_0 F^2(a_0/(2R))\left(Q_{21}^2 + Q_{11}^2\right)}} \tag{14}$$

This condition can be manipulated in order to be expressed in terms of the dimensional parameters in Eq. (4):

$$\frac{\sigma_{\text{def}}^{\max}}{\sigma_{\text{c}}^{\text{b}}} \geq \frac{1}{\sigma_{\text{c}}^{\text{b}}}\sqrt{\frac{G_{\text{c}}^{\text{b}} E}{R}}\sqrt{\frac{G_{1\text{c}}^{\text{i}}}{G_{\text{c}}^{\text{b}}}}\sqrt{\frac{1 + \tan^2(1 - \lambda(G_{2\text{c}}^{\text{i}}/G_{1\text{c}}^{\text{i}})\psi)}{\pi F^2\left(Q_{21}^2 + Q_{11}^2\right)}} \tag{15}$$

where the dimensionless parameters can be identified: γ (or equivalently the inverse of the square root of the dimensionless radius), the ratio of bulk to interface fracture toughness in Mode 1: $G^{\mathrm{i}}_{1\mathrm{c}}/G^{\mathrm{b}}_{\mathrm{c}}$ and the ratio of Mode 2 to Mode 1 interface fracture toughness $G^{\mathrm{i}}_{2\mathrm{c}}/G^{\mathrm{i}}_{1\mathrm{c}}$.

The preferential failure mode will be governed by the ratio in Eq. (4). Thus, dividing Eq. (8) by Eq. (15), the ratio Eq. (4) according to LEFM yields

$$\frac{\sigma^{\max}_{\mathrm{pen}}}{\sigma^{\max}_{\mathrm{def}}} = \sqrt{\frac{G^{\mathrm{b}}_{\mathrm{c}}}{G^{\mathrm{i}}_{1\mathrm{c}}}}\sqrt{\frac{\pi F^2(Q^2_{21}+Q^2_{11})}{1+\tan^2(1-\lambda(G^{\mathrm{i}}_{2\mathrm{c}}/G^{\mathrm{i}}_{1\mathrm{c}})\psi)}} \tag{16}$$

This results in a fully explicit expression of the competition as a function of the dimensionless parameters defined in Section 2. Based on this expression, two possible scenarios can be identified: (i) penetration cases for $\sigma^{\max}_{\mathrm{pen}}/\sigma^{\max}_{\mathrm{def}} < 1$, and (ii) deflection cases $\sigma^{\max}_{\mathrm{pen}}/\sigma^{\max}_{\mathrm{def}} > 1$.

For the sake of brevity, the results of LEFM will be presented and discussed along with the results predicted by FFM in Section 4.2.

4. Coupled criterion of the Finite Fracture Mechanics

Finite Fracture Mechanics (FFM) is based on the assumption that a finite increment of the crack length during the crack initiation or growth. Within this approach, the coupled criterion (CC) (Leguillon, 2002; Cornetti et al., 2006) postulates that the necessary and sufficient condition for crack initiation or growth occurs when the next two conditions are simultaneously fulfilled:

- Stress condition: The stresses over the future crack path reach or exceed a certain level, typically identified with the material strength.
- Energy condition: The released energy during the increment of crack length is enough for the energy required to be dissipated. This energetic balance is similar to that proposed by Griffith (1921) but in an incremental way.

The coupled criterion is particularly useful to predict crack initiation there where Griffith's criterion fails: that is in the vicinity of stress concentrations or weak stress singularities. For these cases, of practical relevance, the Griffith's criterion requires an unrealistic infinite critical load for crack initiation. Thanks to this ability of the coupled criterion, many problems involving crack initiation have been solved in the last two decades for very different material systems and scales, see the comprehensive revisions given in García (2014), Weißgraeber et al. (2016).

Apart from the inherent potential to the accurate prediction of crack initiation events, the coupled criterion can be also particularly useful in order to estimate crack-growth phenomena. In particular, this methodology enables capturing the effect of the size of the process zone as reported by Cornetti et al. (2016). This fact is particularly relevant in this study since the interaction between the process zone, whose size is related to a material characteristic length, and the curvature radius of the weak interface could induce a dependency of the penetration/deflection competition on the curvature radius in situations where the material properties of the system remain unchanged. This is interesting for design purposes and cannot be captured by LEFM in any circumstances.

4.1. Model description

According to the coupled criterion, the remote load $\sigma^{\max}$ for which the crack initiates or propagates is given by the minimum value of the remote load σ fulfilling the two next conditions:

- Stress criterion: The stresses along the future crack path should exceed the strength of the material. This can be written as,

$$\sigma^{\mathrm{cp}}_{\mathrm{eq}}(\sigma^{\mathrm{cp}}(x),\tau^{\mathrm{cp}}(x),\tau_{\mathrm{c}}/\sigma_{\mathrm{c}}) \geq \sigma_{\mathrm{c}},\ \forall x\in[0,\Delta a], \tag{17}$$

  where $\sigma^{\mathrm{cp}}_{\mathrm{eq}}$ is an equivalent stress, homogeneous function of the first order of the normal σ^{cp} and shear τ^{cp} stresses associated to the future crack path. The particular expression for $\sigma^{\mathrm{cp}}_{\mathrm{eq}}$ depends on the material system. The values σ_{c} and τ_{c} respectively stand for the tensile and shear strength at the future crack path. These values will be identified with the interface or bulk strength, depending on the case. The curvilinear coordinate x has its origin at the initial crack tip and runs along the future crack path (in this problem, either straight across the interface or along the interface). The term Δa represents the increment in crack length, which will be a result of the analysis.
- Energy criterion:

$$\underbrace{\int_{a_0}^{a_0+\Delta a} G(a)\mathrm{d}a}_{-\Delta\Pi} \geq \underbrace{\int_{a_0}^{a_0+\Delta a} G_{\mathrm{c}}(a)\mathrm{d}a}_{E_{\mathrm{d}}} \tag{18}$$

  where $-\Delta\Pi$ and E_{d} correspond, respectively, to the energy released and dissipated during the process of increment on crack length, i.e. during the abrupt crack propagation.

The previous criteria can be rewritten as conditions over the critical remote load following the dimensional analysis outlined in Section 2:

- Stress criterion:

$$\frac{\sigma^{\max}}{\sigma_{\mathrm{c}}^{\mathrm{b}}} \geq \max_{x\in(0,\Delta a)} \frac{\sigma_{\mathrm{c}}/\sigma_{\mathrm{c}}^{\mathrm{b}}}{\hat{\sigma}_{\mathrm{eq}}^{\mathrm{cp}}(x,\tau_{\mathrm{c}}/\sigma_{\mathrm{c}})} \tag{19}$$

  where $\hat{\sigma}_{\mathrm{eq}}^{\mathrm{cp}} = \sigma_{\mathrm{eq}}^{\mathrm{cp}}(x)/\sigma$. Note that the condition in (17) imposing that the equivalent stress has to exceed a critical value at every point in $(0, \Delta a)$ is rewritten here as a maximization of this condition over the whole segment $(0, \Delta a)$. This equivalent expression is easier to be implemented for automatic analysis.

- Energy criterion:

$$\frac{\sigma^{\max}}{\sigma_{\mathrm{c}}^{\mathrm{b}}} \geq \frac{1}{\sigma_{\mathrm{c}}^{\mathrm{b}}}\sqrt{\frac{G_{\mathrm{c}}^{\mathrm{b}}E}{R}}\sqrt{\frac{G_{1\mathrm{c}}}{G_{\mathrm{c}}^{\mathrm{b}}}}\sqrt{\frac{\int_{\hat{a}_0}^{\hat{a}_0+\Delta\hat{a}_0}\hat{G}_{\mathrm{c}}(\hat{a})\mathrm{d}\hat{a}}{\int_{\hat{a}_0}^{\hat{a}_0+\Delta\hat{a}_0}\hat{G}(\hat{a})\mathrm{d}\hat{a}}} \tag{20}$$

  where the expressions have been manipulated to make appear the dimensionless parameters and functions introduced in Section 2, adding $\hat{a} = a/R$, $\hat{G}_{\mathrm{c}}(\hat{a}) = G_{\mathrm{c}}(\hat{a})/G_{1\mathrm{c}}$, and $\hat{G}(\hat{a}) = G(a)E/(\sigma^2 R)$. This is the general expression, valid for penetration and deflection. Thus, the terms and functions $G_{1\mathrm{c}}$, $\hat{G}_{\mathrm{c}}(\hat{a})$, $\hat{G}(\hat{a})$ will be particularized for either penetration or deflection below.

According to the coupled criterion, the crack initiation or propagation occurs when the two previous conditions are fulfilled simultaneously, so it can be rewritten by taking the more restrictive, i.e. finding the minimum value of σ fulfilling the two previous conditions simultaneously (i.e. the maximum of the two):

$$\frac{\sigma^{\max}}{\sigma_{\mathrm{c}}^{\mathrm{b}}} = \min_{\Delta\hat{a}}\left(\max\left[\underbrace{\max_{x\in(0,\Delta a)}\frac{\sigma_{\mathrm{c}}/\sigma_{\mathrm{c}}^{\mathrm{b}}}{\hat{\sigma}_{\mathrm{eq}}^{\mathrm{cp}}(x,\tau_{\mathrm{c}}/\sigma_{\mathrm{c}})}}_{s(\Delta\hat{a})};\underbrace{\frac{1}{\sigma_{\mathrm{c}}^{\mathrm{b}}}\sqrt{\frac{G_{\mathrm{c}}^{\mathrm{b}}E}{R}}}_{\gamma}\sqrt{\frac{G_{1\mathrm{c}}}{G_{\mathrm{c}}^{\mathrm{b}}}}\underbrace{\sqrt{\frac{\int_{\hat{a}_0}^{\hat{a}_0+\Delta\hat{a}}\hat{G}_{\mathrm{c}}(\hat{a})\mathrm{d}\hat{a}}{\int_{\hat{a}_0}^{\hat{a}_0+\Delta\hat{a}}\hat{G}(\hat{a})\mathrm{d}\hat{a}}}}_{g(\Delta\hat{a})}\right]\right) \tag{21}$$

This expression can be particularized for the two cases studied here: (i) penetration across the interface, and (ii) deflection along the interface.

First, for penetration scenarios, the crack propagates through the bulk, so $\sigma_{\mathrm{c}} = \sigma_{\mathrm{c}}^{\mathrm{b}}$, and $G_{1\mathrm{c}} = G_{1\mathrm{c}}^{\mathrm{b}}$. In addition, shear stresses are zero along the future crack path:

$$\hat{\sigma}_{\mathrm{eq}}^{\mathrm{cp}}(x,\tau_{\mathrm{c}}/\sigma_{\mathrm{c}}) = \hat{\sigma}^{\mathrm{pen}}(x) \tag{22}$$

Finally, since in this case, the crack grows in pure Mode 1, $G_{\mathrm{c}}^{\mathrm{pen}} = G_{1\mathrm{c}}^{\mathrm{b}}$, so $\hat{G}_{\mathrm{c}}^{\mathrm{pen}} = 1$, and consequently:

$$\int_{\hat{a}_0}^{\hat{a}_0+\Delta\hat{a}}\hat{G}_{\mathrm{c}}(\hat{a})\mathrm{d}\hat{a} = \Delta\hat{a} \tag{23}$$

Thus, the expression in Eq. (21) can be rewritten as:

$$\frac{\sigma_{\mathrm{pen}}^{\max}}{\sigma_{\mathrm{c}}^{\mathrm{b}}} = \min_{\Delta\hat{a}}\left(\max\left[\underbrace{\max_{x\in(0,\Delta a)}\frac{1}{\langle\hat{\sigma}^{\mathrm{pen}}\rangle_{+}(x)}}_{s^{\mathrm{pen}}(\Delta\hat{a})};\underbrace{\frac{1}{\sigma_{\mathrm{c}}^{\mathrm{b}}}\sqrt{\frac{G_{\mathrm{c}}^{\mathrm{b}}E}{R}}}_{\gamma}\underbrace{\sqrt{\frac{\Delta\hat{a}}{\int_{\hat{a}_0}^{\hat{a}_0+\Delta\hat{a}}\hat{G}^{\mathrm{pen}}(\hat{a})\mathrm{d}\hat{a}}}}_{g^{\mathrm{pen}}(\Delta\hat{a})}\right]\right) \tag{24}$$

Note that both $s^{\mathrm{pen}}(\Delta\hat{a})$ and $g^{\mathrm{pen}}(\Delta\hat{a})$ are functions of the elastic solution for stresses, so these terms are universal for this problem and independent of elastic, fracture and strength properties. Similarly to the analysis with LEFM in Section 3, a single dimensionless parameter γ contains the full dependence on the elastic, geometric, fracture, and strength properties.

The values of the stresses $\hat{\sigma}^{\mathrm{pen}}$ and energy release rate $\hat{G}^{\mathrm{pen}}$ are obtained using a set of linear finite element models in ABAQUS, similar to that used in Aranda et al. (2020). The results are presented in Fig. 3. Note that $\hat{\sigma}^{\mathrm{pen}}$ is decreasing from a singular value, corresponding to the value at the crack tip. In contrast, $\hat{G}^{\mathrm{pen}}$ has a finite value for the initial crack length and is always increasing.

Fig. 4 shows the curves corresponding to the condition given by the stress and energy criteria over $\sigma_{\mathrm{pen}}^{\max}/\sigma_{\mathrm{c}}^{\mathrm{b}}$ as a function of the crack length $\Delta\hat{a}$. As can be observed in Eq. (24), the stress criterion is directly given by $s^{\mathrm{pen}}(\Delta\hat{a})$, so the curve is universal for this problem regardless the interface radius. In addition, this curve is increasing, as a consequence of that σ^{pen} is decreasing. Therefore, for penetration, the stress criterion requires a higher remote load if the crack-length increment is larger. In fact, the stress condition goes from zero for $\Delta\hat{a} \to 0^{+}$ (a consequence of the singularity of $\hat{\sigma}^{\mathrm{pen}}$ for $x/R = 0$) to a vertical asymptote in the limit for $\Delta\hat{a} \sim 0.85$, which corresponds to the tension–compression transition in Fig. 3. In contrast with the stress criterion, the curve corresponding to the energy criterion is decreasing, as a consequence of the increasing characteristic of $\hat{G}^{\mathrm{pen}}$. Thus, the energy criterion requires for penetration a lower remote load when the crack length increment is larger. In addition, the curve is translated when the parameter γ is modified. Since this parameter contains the interface radius R, the energy criterion is affected by R, moving downwards the curve when the interface radius is larger. As a consequence, the energy criterion becomes less restrictive for larger R.

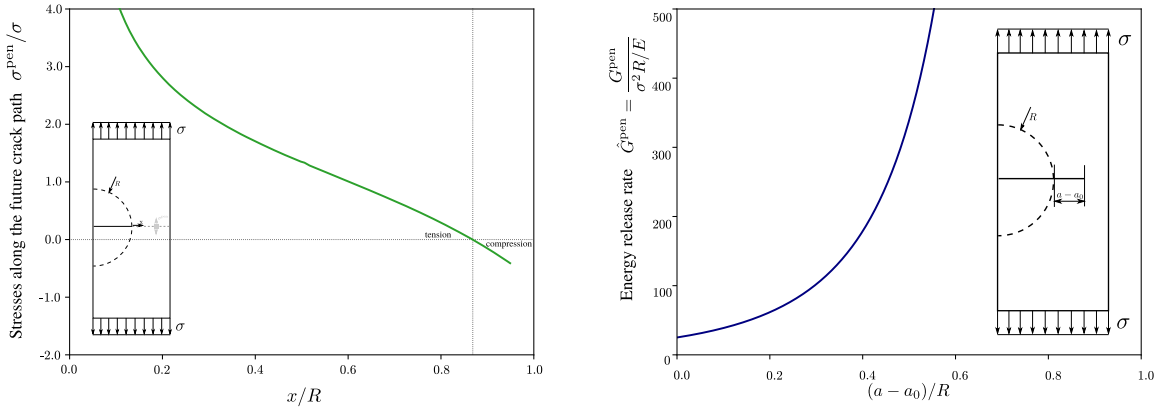

Fig. 3. Stresses along the future crack plane and energy release rate for a crack propagating in the bulk across the interface.

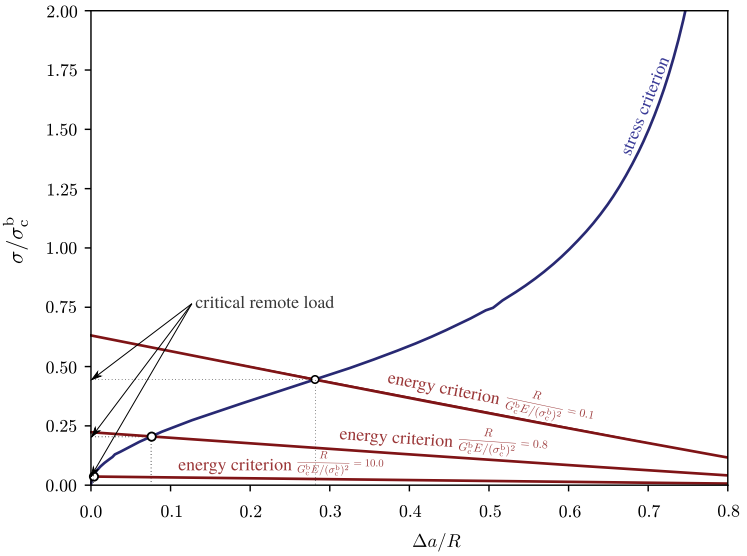

Fig. 4. Stress and energy criteria for crack penetration across the interface.

The coupled criterion postulates that $\sigma^{\max}_{\text{pen}}/\sigma^{\text{b}}_{\text{c}}$ for crack initiation or propagation is given by the minimum fulfilling the two criteria (i.e. the maximum of their respective conditions, see (24)). For penetration, since the stress criterion is increasing with $\Delta\hat{a}$ and the energy criterion is decreasing, the minimum $\sigma^{\max}_{\text{pen}}/\sigma^{\text{b}}_{\text{c}}$ fulfilling the two criteria corresponds to the intersection point of the two criteria. The intersection point is strongly affected by the value of the interface radius as can be observed in Fig. 4.

An analogous analysis can be carried out for deflection by particularizing the general expression in (21) for crack propagating along the interface. In this case, $\sigma_{\text{c}} = \sigma^{\text{i}}_{\text{c}}$, and $G_{1\text{c}} = G^{\text{i}}_{1\text{c}}$. In this case, shear stresses are expected to play a role coupled with tensile stresses, so an equivalent stress $\hat{\sigma}^{\text{def}}_{\text{eq}}$, following García and Leguillon (2012), is defined,

$$\hat{\sigma}^{\text{def}}_{\text{eq}} = \sqrt[m]{\left(\hat{\sigma}^{\text{def}}\right)^m + \left|\hat{\tau}^{\text{def}}\frac{\sigma^{\text{i}}_{\text{c}}}{\tau^{\text{i}}_{\text{c}}}\right|^m} \tag{25}$$

where m is a setting parameter, allowing to recover several classical failure curves, e.g. for $m = 1$, the Mohr–Coulomb criterion is recovered. For this study $m = 2$, which is a typical value for weak interfaces.

In what concerns $\hat{G}_{\text{c}}(\hat{a})$, in this case the fracture mode mixity is expected to be high, thus its influence over the fracture toughness should be taken into account. This influence is approximated following the same phenomenological law used in Section 3 for the LEFM analysis, see (11).

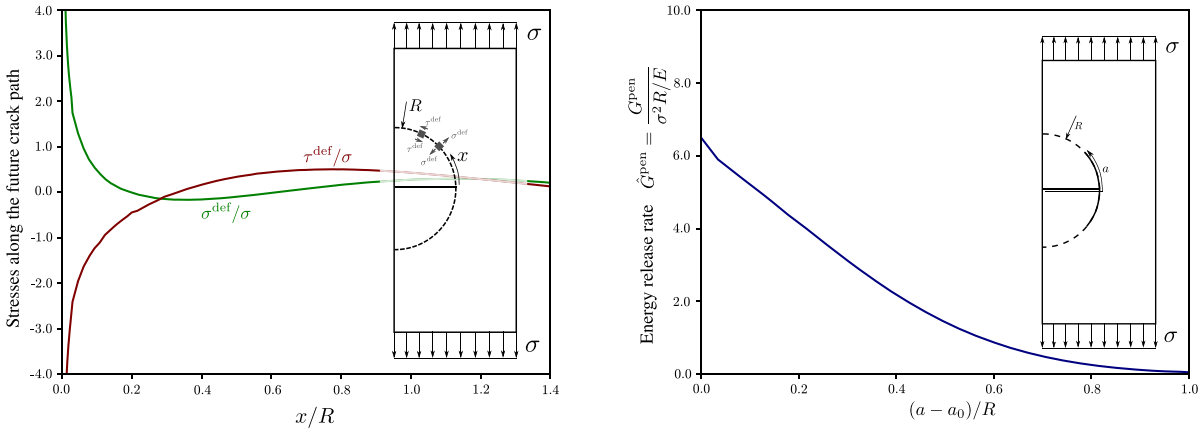

Fig. 5. Stresses along the future crack plane and energy release rate for a crack propagating along the interface.

Then, the expression of the coupled criterion for deflection is written as,

$$\frac{\sigma^{\max}_{\mathrm{def}}}{\sigma^{\mathrm{b}}_{\mathrm{c}}} = \min_{\Delta\hat{a}} \left(\max \left[\underbrace{\min_{x\in(0,\Delta a)} \frac{\sigma^{\mathrm{i}}_{\mathrm{c}}/\sigma^{\mathrm{b}}_{\mathrm{c}}}{\sqrt[p]{\left(\hat{\sigma}^{\mathrm{def}}\right)^p + \left|\hat{\tau}^{\mathrm{def}}\frac{\sigma^{\mathrm{i}}_{\mathrm{c}}}{\tau^{\mathrm{i}}_{\mathrm{c}}}\right|^p}}}_{s^{\mathrm{def}}(\Delta\hat{a})} ; \underbrace{\frac{1}{\sigma^{\mathrm{b}}_{\mathrm{c}}}\sqrt{\frac{G^{\mathrm{b}}_{\mathrm{c}}E}{R}}}_{\gamma} \sqrt{\frac{G^{\mathrm{i}}_{1\mathrm{c}}}{G^{\mathrm{b}}_{\mathrm{c}}}} \underbrace{\sqrt{\frac{\int_{\hat{a}_0}^{\hat{a}_0+\Delta\hat{a}} \left(1+\tan^2(1-\lambda(G^{\mathrm{i}}_{2\mathrm{c}}/G^{\mathrm{i}}_{1\mathrm{c}})\psi)\right)\mathrm{d}\hat{a}}{\int_{\hat{a}_0}^{\hat{a}_0+\Delta\hat{a}} \hat{G}^{\mathrm{def}}(\hat{a})\mathrm{d}\hat{a}}}}_{g^{\mathrm{def}}(\Delta\hat{a})} \right] \right) \tag{26}$$

The values for $\hat{\sigma}^{\mathrm{def}}$, $\hat{\tau}^{\mathrm{def}}$, $\hat{G}^{\mathrm{def}}(\hat{a})$, and ψ are obtained using a similar finite element model to that used in Aranda et al. (2020). All these values could be approximated using different analytical solutions, such as Leblond's one for infinitesimal kinks or Liu and Wei (2021) for finite kinks. In this work, they are extracted using a linear finite element analysis, see Fig. 5. Note that both the tensile σ^{def} and shear τ^{def} stresses are singular at $x/R = 0$ as a consequence of the presence of a crack tip. The monotony of these curves is more complicated than for penetration but it will not be relevant in this case, as will be discussed below. The energy release rate $\hat{G}^{\mathrm{def}}(\hat{a})$ is always decreasing, which makes this curved weak interface an interesting crack arrestor, as observed by Aranda et al. (2020).

Fig. 6 shows the curves corresponding to the condition given by the stress and energy criteria over $\sigma^{\max}_{\mathrm{def}}/\sigma^{\mathrm{b}}_{\mathrm{c}}$ as a function of the crack length increment $\Delta\hat{a}$. As can be observed in Fig. 5, the stresses are singular for $x \to 0^+$ and decreasing for a relevant interval around, so $s^{\mathrm{def}}(\Delta\hat{a} \to 0^+) = 0$. Similarly to the penetration scenario, $\hat{G}^{\mathrm{def}}(\hat{a})$ is finite and non zero for $\Delta\hat{a} = 0$. However, in contrast with the case for penetration, $\hat{G}^{\mathrm{def}}(\hat{a})$ is decreasing. In addition, the fracture mode-mixity increases with $\Delta\hat{a}$. The two previous considerations contribute to the fact that the crack finds more and more difficulty to grow along the interface. As a result, $g^{\mathrm{def}}(\Delta\hat{a})$ is always increasing from a finite value, see Fig. 6.

The coupled criterion postulates that the crack initiates or propagates for the minimum of the maximum of the two curves in Fig. 6. Since the minimum of the two curves is situated at $\Delta\hat{a} = 0$, the increment on crack length is always infinitesimal. Moreover, the stress criterion for this crack length increment is $s(\Delta\hat{a} = 0) \to 0$, which implies that for this length of the crack onset, the stress criterion is always fulfilled. Then, the critical load is given exclusively by the energy criterion, whose minimum is governed directly by the value of the dimensionless parameters γ, $G^{\mathrm{i}}_{1\mathrm{c}}/G^{\mathrm{b}}_{\mathrm{c}}$ and $g^{\mathrm{def}}(\Delta\hat{a})$. The function $g^{\mathrm{def}}(\Delta\hat{a})$, in addition, depends slightly on the ratio of Mode 2 to Mode 1 fracture toughness $G^{\mathrm{i}}_{2\mathrm{c}}/G^{\mathrm{i}}_{1\mathrm{c}}$. The dimensionless parameters $\sigma^{\mathrm{i}}_{\mathrm{c}}/\sigma^{\mathrm{b}}_{\mathrm{c}}$ and $\tau^{\mathrm{i}}_{\mathrm{c}}/\sigma^{\mathrm{i}}_{\mathrm{c}}$ has no influence on the coupled criterion in this case, because they only affect to the stress criterion.

Once the two possible scenarios (penetration and deflection) have been analyzed separately in FFM, the comparison between the critical load required for each one gives the preferential failure mechanism.

4.2. Analysis of FFM and LEFM results

The predictions given by LEFM and FFM are presented in Fig. 7. As discussed previously, the only dimensionless parameters affecting the prediction in LEFM are the ratio of interface to bulk fracture toughness $G^{\mathrm{i}}_{1\mathrm{c}}/G^{\mathrm{b}}_{\mathrm{c}}$ and the ratio of Mode 2 to Mode 1 interface fracture toughness $G^{\mathrm{i}}_{2\mathrm{c}}/G^{\mathrm{i}}_{1\mathrm{c}}$. In the case of the coupled criterion, it is necessary to add the dimensionless radius $R/(EG^{\mathrm{b}}_{\mathrm{c}}(\sigma^{\mathrm{b}}_{\mathrm{c}})^2)$. The dimensionless parameters relating the strength properties, i.e. $\sigma^{\mathrm{i}}_{\mathrm{c}}/\sigma^{\mathrm{b}}_{\mathrm{c}}$ and $\tau^{\mathrm{i}}_{\mathrm{c}}/\sigma^{\mathrm{i}}_{\mathrm{c}}$ have been proved not to affect to the results of either LEFM or FFM. In view of this, the competition between deflection and penetration is presented in the plane $(R/(EG^{\mathrm{b}}_{\mathrm{c}}(\sigma^{\mathrm{b}}_{\mathrm{c}})^2), G^{\mathrm{i}}_{1\mathrm{c}}/G^{\mathrm{b}}_{\mathrm{c}})$ in Fig. 7 with curves for LEFM and FFM which separate the values of the parameters for which penetration or deflection are preferential. The dependence on $G^{\mathrm{i}}_{2\mathrm{c}}/G^{\mathrm{i}}_{1\mathrm{c}}$ is represented using different curves.

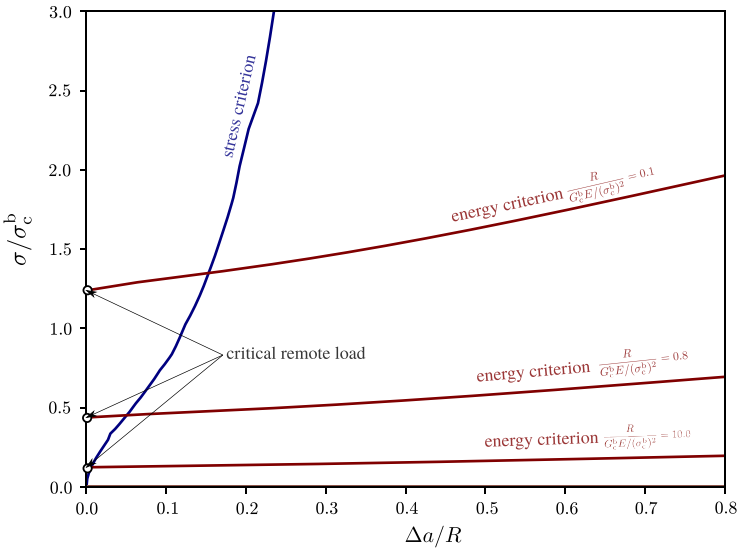

Fig. 6. Stress and energy criteria for crack deflection along the interface.

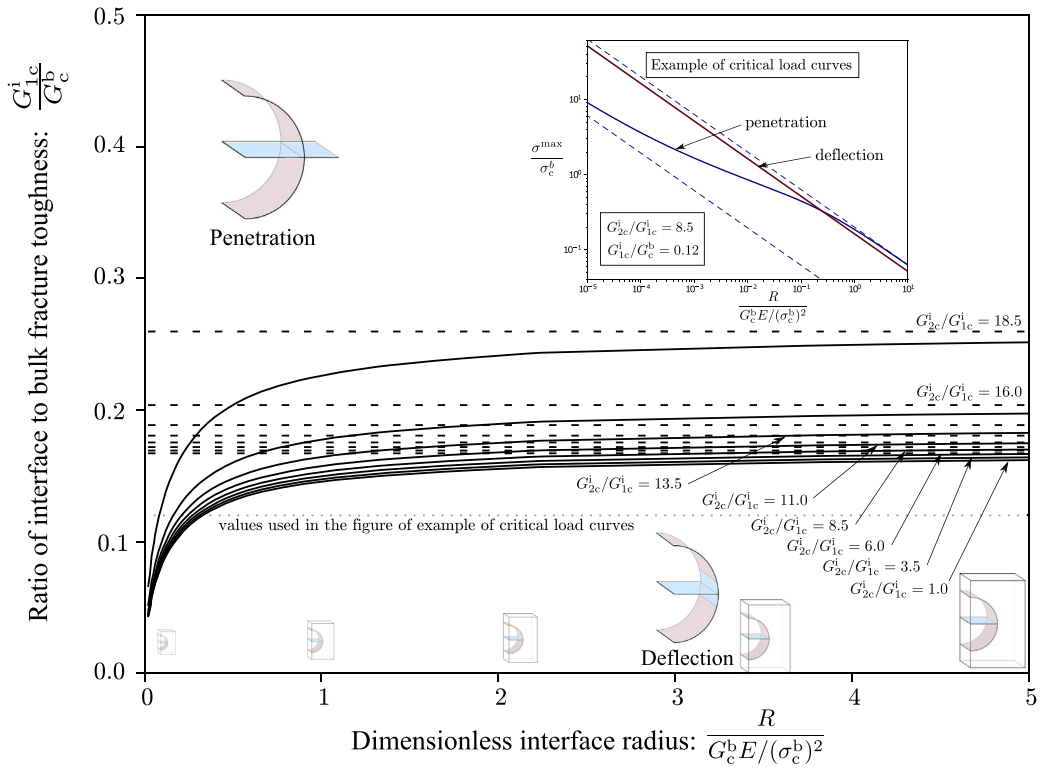

Fig. 7. Transition from deflection to penetration by increasing the interface radio. Solid line: FFM, Dashed line: LEFM.

The results show that the LEFM (dashed lines) predicts a full dependence on the ratio of toughness, which agrees with the prediction of He and Hutchinson (1989). The FFM (solid lines) also predicts that the most relevant parameter for the competition is the ratio of interface to bulk fracture toughness. This result is similar for large crack to the prediction for LEFM (dashed line). However, according to FFM, the interface radius does play a relevant role. In fact, for any situation in the map where deflection is

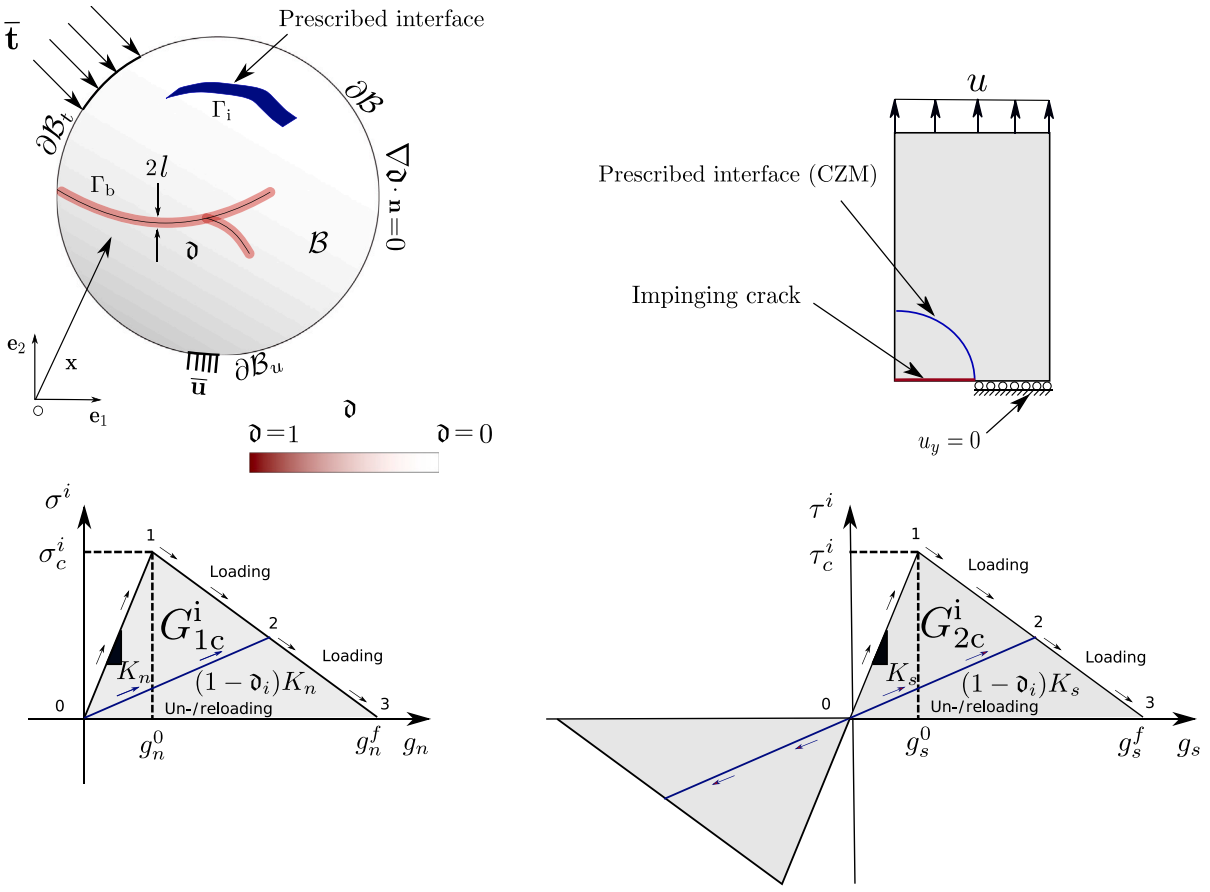

Fig. 8. Combined phase field (PF) and cohesive zone model (CZM) for heterogeneous media. Application to a crack impinging on a curved interface.

predicted, there is always a value of interface radius below which the penetration mechanism becomes preferential. The reason can be understood through the curves of the critical load as the example shown on the top of Fig. 7. In this example, the critical load as a function of the interface radius is plotted for penetration and deflection. From this graph, it can be observed that for deflection the critical load follows the classical LEFM curve. The reason is that, as discussed previously, for deflection the coupled criterion reduces to the energy criterion. In contrast, for penetration, there is a transition when decreasing the interface radius, from the LEFM solution for a large interface radius to a part where the stress criterion has a certain influence to finally a new part again governed asymptotically by the energy criterion. The two extremes are governed by the energy criterion because the stress criterion has a vertical tangent at $\Delta\hat{a} = 0$ and a vertical asymptote at $\Delta\hat{a} \sim 0.85$ as highlighted previously in Fig. 4. As a consequence, the interface radius, as a parameter governing the energy criterion as a factor, promotes this tendency. The transition between the two asymptotic tendencies of the curve corresponding to penetration promotes that below a certain radius, the critical load for penetration becomes lower than the critical load for deflection. In the example, that occurs for $R/(EG_c^b(\sigma_c^b)^2) \sim 0.25$. The potential consequence of this is that the curves separating penetration and deflection in Fig. 4 goes to the origin for $(\sigma_c^b)^2 \to 0$.

5. Computational methodology: combined phase field (PF) and cohesive zone model (CZM) for heterogeneous media

A computational analysis based on a nonlinear finite element (FE) analysis is performed for the present problem combining Phase Field (PF) and Cohesive Zone Model (CZM). This combination, as shown by Paggi and Reinoso (2017), allows the automatic tracking of crack progression at domains containing interfaces. Moreover, the PF and CZM have been proven to capture the size effect inherent in some fracture problems, see e.g. Paggi and Reinoso (2017), Carollo et al. (2017) for PF and Turon et al. (2006), Camanho et al. (2012) for CZM. In this respect, recent investigations have introduced concepts to describe different crack pattern scenarios, e.g. Teichtmeister et al. (2017), Martínez-Pañeda et al. (2018), Quintanas-Corominas et al. (2020), Kristensen and Martínez-Pañeda (2020).

5.1. Model description

Recalling the modeling setting presented by Paggi and Reinoso (2017), the fracture events of a mechanical system containing prescribed weak interfaces can be derived from a potential energy defined as:

$$\Pi(\mathbf{u},\Gamma)=\Pi_{\mathcal{B}}(\mathbf{u},\Gamma_b)+\Pi_{\Gamma_c}(\Gamma)=\underbrace{\int_{\mathcal{B}\setminus\Gamma}\psi^e(\boldsymbol{\varepsilon})\,\mathrm{d}\Omega}_{\text{Bulk elastic energy}}+\underbrace{\int_{\Gamma_b}G_c^b\,\mathrm{d}\Gamma}_{\text{Bulk fracture energy}}+\underbrace{\int_{\Gamma_i}G_c^i\,\mathrm{d}\Gamma}_{\text{Interface fracture energy}}+\Pi_{\text{ext}}(\mathbf{u}), \tag{27}$$

where $\mathbf{u}$ is the displacement field, $\psi^e(\boldsymbol{\varepsilon})$ is the bulk elastic energy density functional governed by the elastic strain tensor $\boldsymbol{\varepsilon}$, G_c^b stands for the bulk fracture energy, G_c^i is the energy dissipated along the prescribed interfaces of the system, and $\Pi_{\text{ext}}(\mathbf{u})$ is the external contribution due to the prescribed surface and body actions. As schematically depicted in Fig. 8, $\mathcal{B}$ refers to an arbitrary body and $\Gamma=\Gamma_i\cup\Gamma_b$ is the interior boundary where the dissipative mechanisms occur, being Γ_i the potential path for interface debonding and Γ_b the interior boundary consequence of the bulk cracking.

Within the context of the PF method for brittle fracture (Bourdin et al., 2008), the fracture bulk energy potential can be approximated by exploiting the Γ-convergence theory as:

$$\int_{\Gamma_c}G_c^b\,\mathrm{d}\Gamma\approx\int_{\mathcal{B}}G_c^b\gamma_{\text{fr}}(\mathfrak{d},\nabla_{\mathbf{x}}\mathfrak{d})\mathrm{d}\Omega. \tag{28}$$

where γ_{fr} is the crack density functional, which depends on the PF variable representing the crack topology and its gradient denoted as $\mathfrak{d}$ and $\nabla_{\mathbf{x}}\mathfrak{d}$, respectively. In turn, the elastic bulk energy potential is modified to account for the smearing of the crack interface by introducing a PF dependency:

$$\int_{\mathcal{B}\setminus\Gamma}\psi^e(\boldsymbol{\varepsilon})\mathrm{d}\Omega\approx\int_{\mathcal{B}}\psi(\boldsymbol{\varepsilon},\mathfrak{d})\mathrm{d}\Omega=\int_{\mathcal{B}}\mathfrak{g}(\mathfrak{d})\psi^e(\boldsymbol{\varepsilon})\mathrm{d}\Omega \tag{29}$$

where ψ is the energy density of the bulk and $\mathfrak{g}(\mathfrak{d})=(1-\mathfrak{d})^2+\mathcal{K}$ is energy degradation function, in which a residual stiffness parameter denoted by $\mathcal{K}$ is introduced for numerical stability proposes.

Within the context of the CZM approach for interface fracture (Turon et al., 2006), the interface fracture energy can be computed through a cohesive law governed by the displacement gaps or jumps between to flanks of the interface when debonding undergoes:

$$\int_{\Gamma_i}G_c^i\,\mathrm{d}\Gamma\approx\int_{\Gamma_i}\psi^i(\mathbf{g}(\mathbf{u});\mathfrak{d}_i)\,\mathrm{d}\Gamma \tag{30}$$

where ψ^i is the interface energy density functional governed by the displacement jump vector $\mathbf{g}$ and the internal state variable describing the damaged state of the interface $\mathfrak{d}_i$. In the context of FE, the displacement jump vector can be obtained using the well-established interface element technology (Schellekens and Borst, 1993).

Steaming from the approximations mentioned above, the potential energy of the system under consideration, Eq. (27), can be rewritten as,

$$\Pi(\mathbf{u},\Gamma)\approx\Pi(\mathbf{u},\mathfrak{d})=\int_{\mathcal{B}}\mathfrak{g}(\mathfrak{d})\psi^e(\boldsymbol{\varepsilon})\mathrm{d}\Omega+\int_{\mathcal{B}}G_c^b\gamma_{\text{fr}}(\mathfrak{d},\nabla_{\mathbf{x}}\mathfrak{d})\mathrm{d}\Omega+\int_{\Gamma_i}\psi^i(\mathbf{g}(\mathbf{u});\mathfrak{d}_i)\,\mathrm{d}\Gamma+\Pi_{\text{ext}}(\mathbf{u})b \tag{31}$$

This approximated form, expressed within the context of the PF and CZM modeling framework, can be solved numerically in an efficient manner and precludes the use of complex algorithms for tracking and re-meshing as the crack events within the bulk and along the prescribe interfaces evolve. Note that Eq. (31) depends upon Γ_i, which identified the prescribed interfaces of the system.

Recalling the variational setting, the fracture events can be predicted under some conditions by minimizing the potential energy, see e.g. Miehe et al. (2010).

Ultimately, Eq. (31) sets the most general form of the potential energy governing the PF+CZM modeling framework, which needs to be particularized according to the consecutive demands of the system analyzed. In this sense, the following constitutive assumptions are used to tackle the problem herein proposed, i.e. the deflection/penetration of cracks in the presence of weak interfaces:

- **Elastic energy density functional**. The constitutive behavior of the bulk region is described with a standard isotropic definition within the infinitesimal deformation setting, which derives from the following Helmholtz free energy function:

$$\psi^{\text{e}}(\boldsymbol{\varepsilon})=\frac{1}{2}\boldsymbol{\varepsilon}:\mathbb{C}:\boldsymbol{\varepsilon}=\frac{1}{2}\lambda\text{tr}^2(\boldsymbol{\varepsilon})+\mu\boldsymbol{\varepsilon}:\boldsymbol{\varepsilon} \tag{32}$$

  where the linear elasticity tensor is defined as: $\mathbb{C}=2\mu\mathbb{I}+\lambda\mathbf{1}\otimes\mathbf{1}$ with the Lame's constants λ and μ. The operators $\mathbb{I}$ and $\mathbf{1}$ respectively denote the fourth and second-order identity tensors, where tr[•] is the trace operator. In the current application, the positive–negative decomposition of the strain energy usually introduced in PF models is not considered because the prescribed remote tensile loading under quasi-static conditions precludes the crack closure effect.
- **Interface energy density functional**. The constitutive response of the interface region is assumed to have a cohesive response, described by a well-established bilinear Traction Separation Law (TSL) built-in in ABAQUS. For the 2D scenario herein studied, this assumption means that the fracture of the interface is governed by a phenomenological model relating the normal and shear displacement jumps across the interface, g_n and shear g_s, with the corresponding components of the traction vector

acting on it, σ^i and τ^i, respectively. Hence, the response only accounts for fracture Modes 1 and 2 as shown in see Fig. 8. Then, the TSL is simply defined as:

$$\sigma^i = (1-\mathfrak{d}_i)K_n \langle g_n \rangle_+ + K_n \langle g_n \rangle_- \tag{33}$$

$$\tau^i = (1-\mathfrak{d}_i)K_t g_s \tag{34}$$

where $\mathfrak{d}_i$ is the state damage variable tracking the cracking of the interface, being $\mathfrak{d}_i = 0$ bonded state (undamaged) and $\mathfrak{d}_i = 1$ debonded state (damaged), while it ensures the irreversible character of the fracture process (Turon et al., 2006). In line with (Zambrano et al., 2022), it is worth noting that no explicit coupling between the PF for bulk fracture and the CZM for interface cracks is herein considered.

Finally, a quadratic fracture propagation criterion for mixed-mode fracture conditions adopted (Reinoso and Paggi, 2014), relating the Modes 1 and 2 energy release rates, G_1^{i} and G_2^{i}, with the corresponding fracture toughness values, $G_{1\mathrm{c}}^{\mathrm{i}}$ and $G_{2\mathrm{c}}^{\mathrm{i}}$:

$$\left(\frac{\langle G_1^{\mathrm{i}} \rangle_+}{G_{1\mathrm{c}}^{\mathrm{i}}}\right)^p + \left(\frac{G_2^{\mathrm{i}}}{G_{2\mathrm{c}}^{\mathrm{i}}}\right)^p = 1 \tag{35}$$

where $\langle \bullet \rangle_\pm$ is the Macaulay brackets supporting the crack closure effects associated with the Mode 1 opening. In the present work, the interface properties satisfy: $G_{2\mathrm{c}}^{\mathrm{i}}/G_{1\mathrm{c}}^{\mathrm{i}} = 7.71$ and $\sigma_{\mathrm{c}}^{\mathrm{i}}/\tau_{\mathrm{c}}^{\mathrm{i}} = 1$. The exponent $p = 2$ is chosen, but some computations were carried out for $p = 4$ without finding a strong influence.

- **Crack density functional**. The crack density functional describing the topology of the crack used in this work is the quadratic model, known as AT1, introduced by Bourdin et al. (2000) for brittle fracture:

$$\gamma_{\mathrm{fr}}(\mathfrak{d}, \nabla_{\mathbf{x}}\mathfrak{d}) = \frac{3}{8}\left(\frac{\mathfrak{d}}{\ell} + \ell \left|\nabla_{\mathbf{x}}\mathfrak{d}\right|^2\right) \tag{36}$$

where $\ell > 0$ is the regularization length. Although in the original conception of the PF model ℓ is essentially a numerical parameter, Tanné et al. (2018) showed that it can be linked with the classical material's characteristic length ℓ_{ch} in order to match the nominal material's strength σ_c for a given material properties, namely: fracture toughness G_c, Young's modulus E, and Poison coefficient ν or stress intensity factor K_{Ic}. For the AT1 model, the heuristic expression of interest is given by

$$\sigma_{\mathrm{c}}^{\mathrm{b}} = \sqrt{\frac{3G_{\mathrm{c}}^{\mathrm{b}}E'}{8\ell}} \implies \ell = \frac{3}{8}\frac{G_{\mathrm{c}}^{\mathrm{b}}E'}{\left(\sigma_{\mathrm{c}}^{\mathrm{b}}\right)^2} \tag{37}$$

where $E' = E$ for current plane-stress scenarios. According to previous investigations, it is noting that AT1 version of PF model can retrieve size effects and transition flaw size for enough refined meshes. In this sense, Tanné et al. (2018), Kristensen et al. (2021) showed that the PF basic formulation agrees with Griffith's criterion for large cracks while predicting the smooth transition to the strength-dominated failure as the crack size decreases below the transition flaw size.

As mentioned above, the influence of the dimensionless design parameters on the crack penetration/deflection competition in the presence of weak interfaces formulated in the context of the PF+CZM stemming from Eq. (31), is herein spatially discretized through the FEM (Quintanas-Corominas et al., 2020). In this regard, the linearized form of the problem is implemented in ABAQUS, following a well-established strategy using a UEL and a staggered solution scheme, see e.g. Wu and Huang (2020).

Remark 1. The Dimensional Analysis presented in Section 2 can be applied to this model. Nevertheless, it is required to include *a priori* two characteristic lengths which appeared in the computational model and were not included in the general Dimensional Analysis:

- The regularization length ℓ. In a PF general formulation, this is a numerical parameter. However, in this case, the parameter ℓ can be associated with the material properties through Eq. (37), so it is not an independent parameter.
- The characteristic element size. This length should not affect the results if the mesh is adequately designed. This point is discussed in the sequel.

Focusing on the problem of interest, the computational domain concerns the upper half part of the original geometry thanks exploitation of symmetry conditions, resulting in a rectangular plate of 150×50 mm with a quarter circle with radius 25 mm embedded as shown in Fig. 8. The weak interface is situated in the perimeter of this quarter circle. In turn, the initial crack is defined at the left half part of the bottom boundary by prescribing a traction-free condition along the corresponding edge. This approach to introducing a crack in PF (so-called geometric crack) has been shown to overestimate the critical load for propagation, see Kristensen et al. (2021). However, for several cases of the present study, the strategy based on prescribing $\mathfrak{d}$ cannot be used when ℓ is related to the process zone because the initial damaged region could be very large (and therefore providing meaningless predictions). The present problem is particularly affected by this limitation since the size of the model plays a key role in capturing the effect of the curvature radius. The initial crack tip intersects between the weak interface and the bottom boundary, corresponding to the bottom edge's center point. According to a preliminary study of the fields near the crack tip, this setup has been selected to mitigate the possible influence of the lateral boundaries. A symmetry condition is prescribed at the part of the boundary which is still intact. Although this condition is not fully compatible with the expected phase field near the symmetry line because $\partial\mathfrak{d} \neq 0$ where $\mathfrak{d} = 1$, several previous investigations within the related literature have employed this approach showing a good accuracy, see e.g. Tanné et al. (2018) and the references therein.

Regarding the FE mesh, the bulk region is discretized by 161,150 quadrilateral elements with linear interpolation of the displacements and the phase field variable, with a minimum size of $h = 0.125$ mm in the expected crack path and complying with the recommendation of Miehe et al. (2010) of having enough elements in the region affected by the regularization length ℓ. This condition is fulfilled here, even if the mesh remains unchanged. Since the maximum $R/(EG_c^b/(\sigma_c^b)^2)$ is set equal to 5.0 and R is kept fixed with the mesh, the minimum ℓ corresponds to 1.875 mm, then fulfilling $h/\ell < 0.2$ in the worst case scenario. The weak interface region is discretized by 256 interface elements with a minimum in-plane size of 0.15 mm, satisfying the minimum requirements associated with the fracture process zone identified by Turon et al. (2006). Finally, concerning the loading conditions, a monotonic increasing displacement u upon failure is prescribed on the upper edge boundary by employing a displacement-control scheme. It is worth noting that the distance between the upper edge and the crack tip is far enough for the displacement-controls scheme, and therefore providing similar results to those associated with the uniform remote stress loading conditions (which corresponded to the applied loading conditions for the LEFM and FFM models).

The modeling framework and the computational domain described previously set the baseline configuration for the current dimensional analysis detailed above. In the FE context, it has twofold characteristics that make it a powerful tool for parametric studies involving size effects: (i) the reduction of the number of simulations to be conducted without loss of universality on the results and (ii) the proper evaluation of the size effect of the radius without modifying the mesh between models, avoiding mesh-dependency of the results. Thus, the characteristic element sizes of the baseline mesh have been selected for the most restrictive scenario in order to prevent any interference between the fracture process zones and the regularization PF length. Some tests have been performed to check the accuracy of this strategy for some extreme values of the radius. The results showed relative differences lesser than 0.01% in the worst case.

5.2. Numerical results

A total set of 600 models have been computed varying the three dimensionless parameters governing the failure mechanism: the ratios of strength σ_c^i/σ_c^b and fracture toughness G_{1c}^i/G_c^b; and the dimensionless radius $R/(EG_c^b/(\sigma_c^b)^2)$.

Fig. 9 shows some illustrative examples of the behavior observed in the computational results. In particular, it is interesting to remark the influence of the dimensionless parameter on the damaged zone and its progression beyond the penetration/deflection competition. In this graph, representative points are labeled as a and b for a clear identification in the subsequent discussion. Moreover, the shaded region in Fig. 9 is introduced due to the minor significance of the FE predictions since the bulk-damaged regions did not correspond to localized fracture phenomena.

- For $\sigma_c^i/\sigma_c^b = 4.0$, the overall numerical results render penetration scenarios regardless the value of the other parameters. This result agrees with the observations by Zambrano et al. (2022) for straight interfaces studied with a PF+CZM with some differences in the numerical modeling and implementation. The explanation for this will be discussed in Section 6. This trend holds with the exception of a very low value of $R/(EG_c^b/(\sigma_c^b)^2)$ and G_{1c}^i/G_c^b leading to deflection cases. The contour map of the damage variable shows a clear penetration for the case b, corresponding to intermediate values of the ratio of fracture toughness G_{1c}^i/G_c^b and the dimensionless radius $R/(EG_c^b/(\sigma_c^b)^2)$. In this case, the crack progression is clearly recovered by the phase field, while the interface remains intact. This result is a direct consequence of the threshold role associated to the strength criterion in the cohesive model. For the case a, where the radius is very small, crack deflection is observed. However, the damage variable in the bulk reaches a very high value but with a very diffused area, affecting the whole bulk domain. The interaction between the cohesive damage along the interface and this diffusive region presents a difficulty in combining CZM and PF when the latter is used beyond the asymptotic approach of LEFM for $\ell \to 0$, justifying the definition of the aforementioned shaded region in the diagrams as will be discussed for $\sigma_c^i/\sigma_c^b = 1.0$.
- For $\sigma_c^i/\sigma_c^b = 1.5$ and 2.0, the general trend also complies with penetration scenarios, except for very low values of G_{1c}^i/G_c^b and/or $R/(EG_c^b/(\sigma_c^b)^2)$. For instance, for the case a, crack deflection is predicted, showing a clear zone debonded at the interface closer to the crack tip. Note however that for this particular case a, a concomitant small damaged zone can be observed at the vicinity of the crack tip below the interface. This suggests that this case lies within the limit of the transition between penetration and deflection cases, which is confirmed by the situation of the corresponding point in the figure. In fact, the case b corresponds to a nearby case with penetration where only $R/(EG_c^b)$ was increased, highlighting the influence of this parameter.
- For $\sigma_c^i/\sigma_c^b = 1.0$, the corresponding predictions are very similar to the previous configurations. The illustrative cases were chosen here in order to provide further insight into the analysis of the effect of the dimensionless radius $R/(EG_c^b/(\sigma_c^b)^2)$. Both points a and b correspond now to cases where deflection is predicted. However, the computed damaged zone within the specimen is very different from each other. Focusing on the damaged region in the bulk the denominated case a recalls a very diffuse damaged zone, whereas, conversely, the damaged zone for the case b is constrained to a very small zone of the bulk below the crack tip. The reason for this difference in the bulk-damage predictions is attributed to the variation of the dimensionless radius $R/(EG_c^b/(\sigma_c^b)^2)$, which can be interpreted as the inverse of the ratio of a material characteristic length $EG_c^b/(\sigma_c^b)^2$ to the curved interface radius R and associated to the length of the process zone. Thus, the inverse of the dimensionless radius characterizes the relative size of the process zone on the bulk with respect to the problem geometry. While these considerations correspond only to the process zone of the bulk because the radius is normalized with the bulk properties, an analogous dimensionless parameter could be obtained by combining $R/(EG_c^b/(\sigma_c^b)^2)$ with σ_c^i/σ_c^b and G_{1c}^i/G_c^b, giving a parameter characterizing the contrast between the curved interface radius and the estimation of the size of the process zone at the interface. Since between the cases a and b, σ_c^i/σ_c^b and G_{1c}^i/G_c^b remain fixed, the variation on this new parameter is

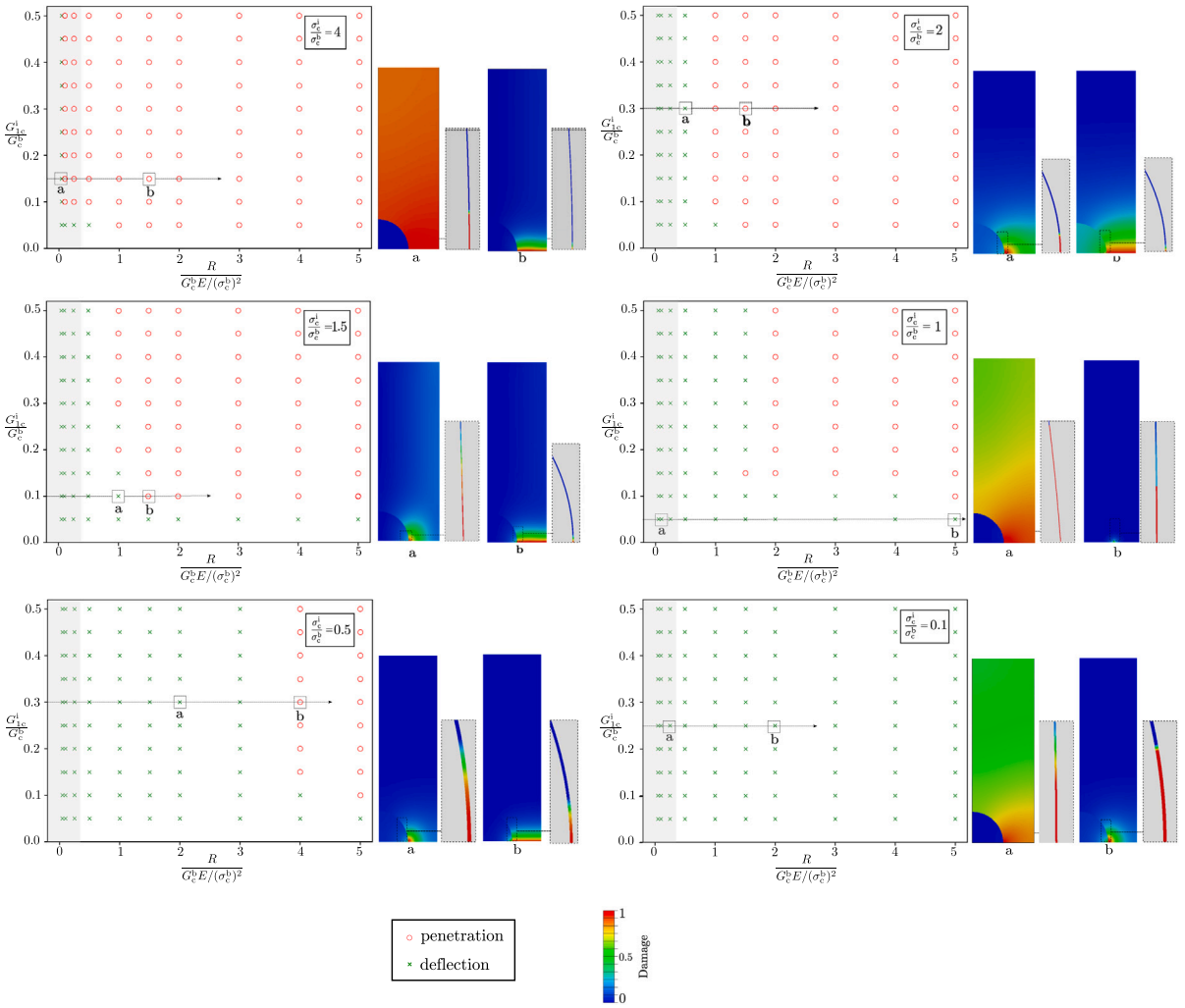

Fig. 9. Computational results extracted from the models combining the Phase Field approach and Cohesive Zones. Illustrative examples of the different behavior observed. Gray-shaded areas correspond to results with large ℓ compared with the radius.

equivalent to the variation of $R/(EG_c^b/(\sigma_c^b)^2)$. As a consequence, the process zone is also relatively much larger at the interface for case a than for case b. Both process zones, at the bulk and at the interface modulate the relevance of the curvature of the interface over the result of the competition, and therefore one can conclude that: a larger process zone yields relevance to the part of the interface farther from the crack tip.

- For $\sigma_c^i/\sigma_c^b = 0.5$, the situation is qualitatively similar to the previous case ($\sigma_c^i/\sigma_c^b = 1$), but with deflection scenarios being predicted for a much larger range of values of the dimensionless parameters. In particular, it is interesting to remark the clear relevance of the interface radius on the penetration/deflection competition. The cases a and b are very close to each other, with the only difference on the value of $R/(EG_c^b/(\sigma_c^b)^2)$.
- For $\sigma_c^i/\sigma_c^b = 0.1$, the situation is the opposite to that found for $\sigma_c^i/\sigma_c^b = 4.0$. In this case, crack deflection is predicted for the whole range of values studied for G_{1c}^i/G_c^b and $R/(EG_c^b/(\sigma_c^b)^2)$. This fact highlights again that for the computational strategy of combining PF and CZM, the ratio of strengths between both methodologies is the key parameter, as discussed previously for $\sigma_c^i/\sigma_c^b = 4.0$ and already described and explained by Parmigiani and Thouless (2006), Zambrano et al. (2022) for similar models. For the sake of illustration, damaged patterns are plotted for cases a and b, corresponding to cases where deflection is predicted. However, the damaged zones of the bulk are very different from each other. For case a, a very diffuse damaged zone is predicted, whereas in case b, the damaged zone is constrained to a very small zone of the bulk below the crack tip.

Previous considerations on the analysis of the role of the different parameters that govern the mechanical response of the system can be also observed in Fig. 10. This graph presents a summary of the prediction of this model about the penetration/deflection competition, showing the influence of the three dimensionless parameters studied. From this plot, it becomes clear the fact that the ratio of strengths σ_c^i/σ_c^b represents the key parameter in the current numerical predictions.

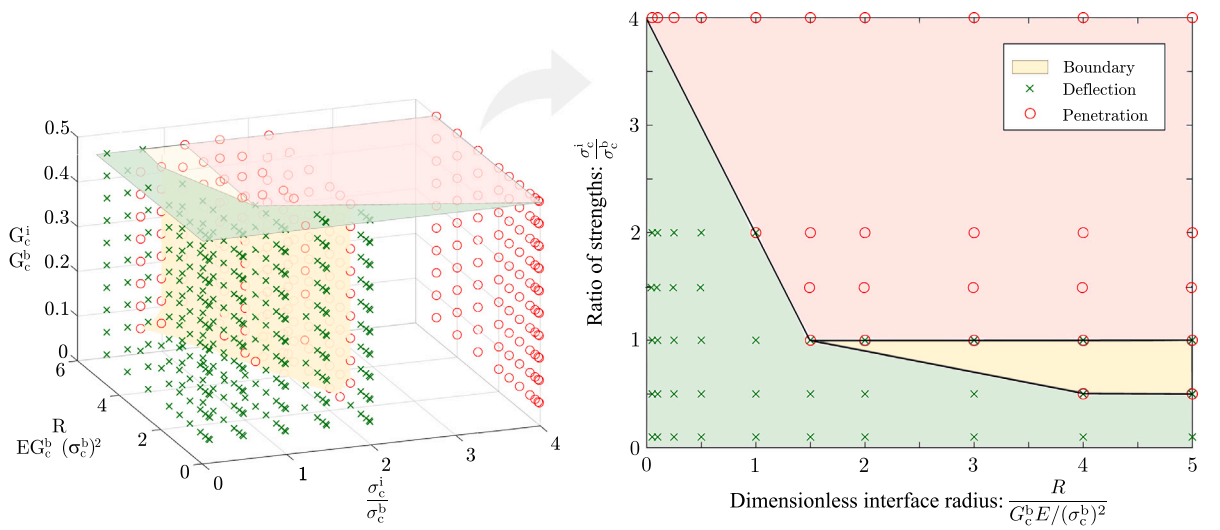

(a) 3D representation of the three parameters under consideration and a plan projection comparing the dimensionless interface radius, $R/(EG_c^b/(\sigma_c^b)^2)$, respect to the strengths ratio, σ_c^i/σ_c^b.

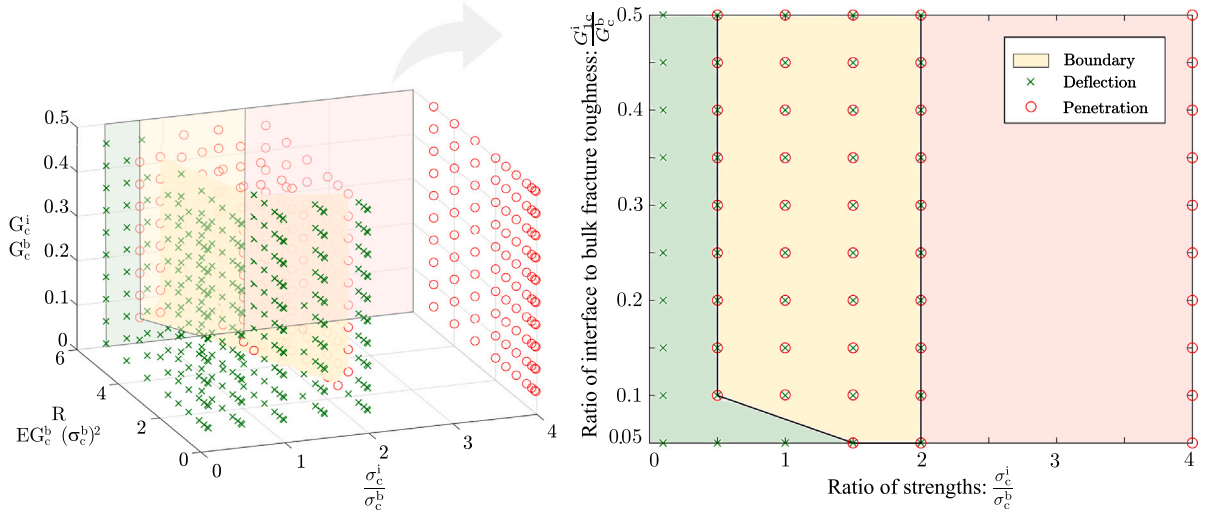

(b) 3D view of the three parameters studied and a elevation projection representing the ratio of strengths σ_c^i/σ_c^b with respect to the ratio of interface to bulk fracture toughness G_{1c}^i/G_c^b

Fig. 10. Penetration/deflection competition. Results predicted by the approach based on combining Phase Field and Cohesive Zone Model.

6. Comparison and discussion

This section presents a critical comparison between the present predictions using the three approaches presented previously (namely, LEFM, FFM and combined PF-CZ). In particular, the comparison focuses on how the governing mechanical parameters of the system affect to the results of the penetration/deflection competition, pinpointing the physical sense of the predictions.

Fig. 11 presents a set of maps containing the prediction of the three approaches. For the sake of simplicity, only the results from the Phase Field + Cohesive Zone Model analysis are represented with different color symbols, whereas the predictions by LEFM and FFM are presented by dashed and solid lines, respectively, separating deflection from penetration scenarios. For these two approaches, above and below this line always correspond to penetration and deflection, respectively.

Table 1 summarizes the effect of the dimensionless parameters on the penetration/deflection competition. In what follows the effect of each dimensionless parameter is discussed:

Effect of the ratio of fracture toughness G_{1c}^i/G_c^b. Based on the previous results, it was clearly observed that the effect of the ratio of fracture toughness is the governing parameter that rules the deflection/penetration competition according to LEFM. Thus, when G_{1c}^i/G_c^b increases the crack tends to penetrate instead of deflecting. Under their assumptions of infinitesimal crack growth and

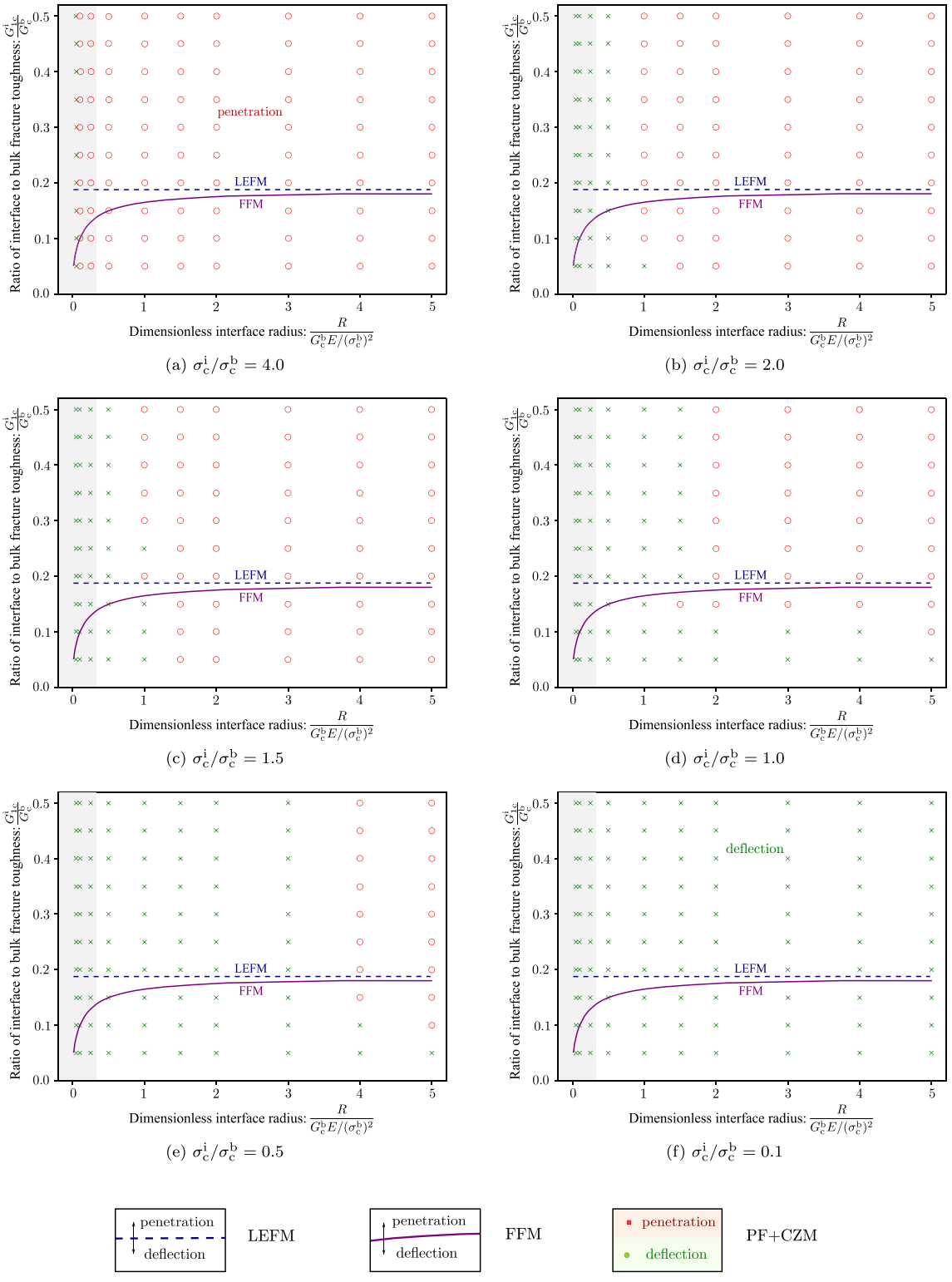

Fig. 11. Comparison between the predictions given for the different approaches for the penetration/deflection competition. Gray-shaded areas corresponds to PF+CZM results with large ℓ compared with the radius.

Table 1
Influence of the dimensionless parameter on the penetration/deflection competition. p: Increasing this parameter promotes crack penetration. d: Increasing this parameter promotes crack deflection. =: This parameter has no effect on the penetration/deflection competition.

	$G^{i}_{1c}/G^{b}_{c}\uparrow$	$\sigma^{i}_{c}/\sigma^{b}_{c}\uparrow$	$R/(EG^{b}_{c}/(\sigma^{b}_{c})^2)\uparrow$
LEFM	Penetration	No influence	No influence
FFM	Penetration	No influence	Deflection
PF+CZM	Penetration	Penetration	Penetration

vanishing process zone, the parameter G^{i}_{1c}/G^{b}_{c} modulates if penetration or deflection is more preferential exclusively from an energetic point of view. Finite Fracture Mechanics agrees qualitatively with this behavior, so that a larger value for G^{i}_{1c}/G^{b}_{c} promotes crack penetration. The reason is that FFM is based partially on optimizing the energetic balance. However, the prediction of a process zone and the need of fulfilling a stress criterion in FFM modulates the influence of G^{i}_{1c}/G^{b}_{c}. Concerning PF + CZM the behavior is qualitatively similar to the two previous methodologies in what respect to G^{i}_{1c}/G^{b}_{c}, but much more ruled by the other parameters. In fact, it is only particularly relevant for $\sigma^{i}_{c}/\sigma^{b}_{c}=1$.

Effect of the ratio of strengths $\sigma^{i}_{c}/\sigma^{b}_{c}$. The predictions corresponding to the effect of $\sigma^{i}_{c}/\sigma^{b}_{c}$ are more diverse among the three approaches under consideration. First, as expected, LEFM analysis are independent upon this ratio since the strength does not play any role in LEFM. Conversely, for FFM results, where stress and energy criteria are simultaneously fulfilled, it would be expected that $\sigma^{i}_{c}/\sigma^{b}_{c}$ could affect the results on penetration/deflection competition. However, for this particular problem, the decreasing value of the stresses when advancing along the interface yields that FFM predicts a vanishing length of the crack onset when it occurs at the interface, see Section 4 for a detailed discussion. As a consequence, for the interface crack onset, the solution of FFM matches with that of LEFM, removing the influence of $\sigma^{i}_{c}/\sigma^{b}_{c}$. In contrast, the PF+CZM approach predicts a strong effect of the ratio of strengths on the penetration/deflection competition. The reason is the triggering role of the strength on the cohesive zone model (very particularly for the bilinear cohesive law used) and partly on the phase field. This effect is particularly relevant for short cracks, being expected that for long cracks the fracture energy plays a role. However, as described and explained by Parmigiani and Thouless (2006), Zambrano et al. (2022) for CZM+CZM and PF+CZM models respectively, the deflected crack in most situations is short enough to avoid the influence of the toughness. Thus, the deflection/penetration can be preferential according to PF+CZM even if the solution is not preferential from the energetic point of view. Concerning the influence of the ratio τ_{ci}/σ_{ci}, LEFM and FFM do not predict any influence in line with the independence of the strength properties. However, for PF+CZM some numerical tests have been performed, showing that the influence is similar to that of $\sigma^{i}_{c}/\sigma^{b}_{c}$, i.e. promoting penetration.

Effect of the dimensionless radius $R/(EG^{b}_{c}/(\sigma^{b}_{c})^2)$. The interface radius is the parameter which can be tailored more easily as a design parameter in the application of curved weak interfaces as crack arrestors. The LEFM approach does not predict any influence of this parameter on the competition. The cause is that LEFM is based on an infinitesimal crack advance and on assuming a vanishing process zone. Under this hypothesis, the crack deflection along the interface is always an infinitesimal crack deviation of 90°, without any effect of the curvature. In contrast, the FFM approach does predict a certain process zone, understanding that in the sense of the analysis as a zone of finite length where the stress state is taken into account. The length of this process zone in FFM is strongly affected by the analysis itself. In particular, in this case, this kind of process zone predicted by FFM along the interface is vanishing, whereas the process zone along the bulk is strongly affected by the problem parameters. This contrast produces an influence of the radius, i.e. when this is reduced the crack penetration is promoted. The effect of the radius is predicted to be much more strong by the PF + CZM approach. In this case, a process zone is also predicted, being very related with the material characteristic length at the bulk $EG^{b}_{c}/(\sigma^{b}_{c})^2$ and at the interface $EG^{i}_{1c}/(\sigma^{i}_{c})^2$. As a consequence, the radius has a strong effect on the penetration/deflection competition, as can be observed in the preliminary experimental results reported in Table 1.

7. Concluding remarks

The ability of a weak curved interface to deviate a crack was studied using three different approaches: Linear Elastic Fracture Mechanics (LEFM), Finite Fracture Mechanics (FFM), and a combination of Phase Field and Cohesive Zone Model (PF+CZM). These methodologies were employed to evaluate potential penetration/deflection competition in specimens with a prescribed curved interface.

Current results based on LEFM, FFM and PF+CZM agree general trends regarding the expected effect of the ratio of interface to bulk fracture toughness. However, these methods present significant differences on corresponding predictions with reference to the effect of the ratio of interface to bulk strength. Thus, on the one hand, LEFM and FFM predicted that $\sigma^{i}_{c}/\sigma^{b}_{c}$ had no effect on the potential failure scenarios, whereas, on the other hand, PF+CZM yielded to simulation results where an increasing value for $\sigma^{i}_{c}/\sigma^{b}_{c}$ promoted strongly the penetration of the primary crack on the adjacent body. Finally, with reference to the effect of the ratio $R/(EG^{b}_{c}/(\sigma^{b}_{c})^2)$, current results rendered that this parameter had no influence on the crack path for LEFM, but governing the failure characteristics in FFM ($R/(EG^{b}_{c}/(\sigma^{b}_{c})^2)\uparrow$ deflection) and PF+CZM ($R/(EG^{b}_{c}/(\sigma^{b}_{c})^2)\uparrow$ penetration).

In addition to the previous main conclusions on the corresponding results, it is worth to mention that the complexity of the models for this problem in terms of computational cost is very diverse between the chosen methods. Thus, while LEFM can be

applied using an explicit equation, the use of FFM required the solution of some simple nonlinear equations. In contrast, the current numerical technique PF+CZM needed the computation of nonlinear finite element models with relatively fine mesh (leading to computation times of around 1 h per model).

From a more physically sound point of view, current analysis pinpointed the relevance of the process zone on the prediction about the penetration/deflection competition in curved interfaces, showing that the effect of the radius was strongly affected by the assumptions made by the different approaches. In this sense, beyond the motivation of the application itself, this problem is an interesting laboratory for testing these three approaches. This is highlighted by the differences found between PF+CZM and FFM, which are *a priori* conceptually equivalent to each other, if the regularization length ℓ corresponds to a material-based parameter, as has been assumed in this work. However, there are some differences that are key for the results presented here and are related to how PF and FFM deal with the finite length differently. Whereas the finite length on which the PF approach is relied on is now given by material properties, in FFM this finite length is a result stemming from the corresponding analysis, see e.g. Leguillon (2002). The length scale affecting to the fracture behavior plays an essential role here because it can interact with the curvature radius, as observed in the results, then promoting divergent results in some cases, as observed here. Moreover, current analysis assumed that the initial crack is much larger than the deflected or penetrated finite crack. However, in some situations, the initial crack length could be similar to the finite crack, and it could affect the value of the energy release rate as shown by Liu and Wei (2021).

Finally, from a qualitative point of view, it is noted that FFM predictions are more in line with the preliminary experiments that motivated the realization of this study (see Fig. 1).

Future experiments are planned with specimens with varying interface radii, in order to evaluate the assumptions made by the three approaches used herein. Potential experimental campaigns are also considered for the assessment of cracking phenomena of multi-material specimens with the presence of weak curved interfaces. As final comment, note that this work focuses on cracks reaching the interface at the symmetry line and perpendicular to the interface. Deflection angle could affect significantly the results and could be the objective of future works.

Declaration of competing interest

The authors declare that they have no known competing financial interests or personal relationships that could have appeared to influence the work reported in this paper.

Data availability

Data will be made available on request.

Acknowledgments

The authors would like to express their deepest gratitude to Prof. Vladislav Mantič (Universidad de Sevilla, Sevilla, Spain) for his relevant contribution through great discussions.

The authors also want to acknowledge Profs. Marco Paggi (IMT Lucca, Lucca, Italy) and Davide Bigoni (Universita di Trento, Trento, Italy) for encouraging this research, and Eng. Alejandro Estefani for his assistance in accurate meshing.

The authors appreciate the financial support of the Junta de Andalucía through the Consejería de Economía y Conocimiento, and European Regional Development Fund (Project P20-00595). The authors acknowledge the support of the Spanish Ministry of Science and Innnovation (Projects PGC2018-099197-B-I00, PID2020-117001GB-I00 and TED2021-131649B-I00). IGG and JR appreciates the support of the funding received from the Marie Skłodowska-Curie grant agreement No. 101086342 – Project DIAGONAL (Ductility and fracture toughness analysis of functionally graded materials; HORIZON-MSCA-2021-SE-01 action).

References

Alam, M., Parmigiani, J., Kruzic, J., 2017. An experimental assessment of methods to predict crack deflection at an interface. Eng. Fract. Mech. 181, 116–129.
Ambati, M., Gerasimov, T., De Lorenzis, L., 2015. Phase-field modeling of ductile fracture. Comput. Mech. 55, 1–32.
Amestoy, M., Leblond, J., 1992. Crack paths in plane situations—II. Detailed form of the expansion of the stress intensity factors. Int. J. Solids Struct. 29 (4), 465–501.
Aranda, M.T., García, I.G., Reinoso, J., Mantič, V., 2022. Experimental evaluation of the similarity in the interface fracture energy between PMMA/epoxy/PMMA and PMMA/epoxy joints. Eng. Fract. Mech. 259, 108076.
Aranda, M.T., García, I.G., Reinoso, J., Mantič, V., Paggi, M., 2020. Crack arrest through branching at curved weak interfaces: An experimental and numerical study. Theor. Appl. Fract. Mech. 105, 102389.
Banks-Sills, L., Travitzky, N., Ashkenazi, D., 2000. Interface fracture properties of a bimaterial ceramic composite. Mech. Mater. 32 (12), 711–722.
Barenblatt, G.I., 1962. The mathematical theory of equilibrium cracks in brittle fracture. Adv. Appl. Mech. 7, 55–129.
Barenblatt, G.I., Cherepanov, G.P., 1961. On brittle cracks of longitudinal shear. Journal of Applied Mathematics and Mechanics 25 (6), 1654–1666 (in Russian).
Bažant, Z.P., Kasemi, M.T., 1990. Determination of fracture energy, process zone longth and brittleness number from size effect, with application to rock and conerete. Int. J. Fract. 44, 111–131.
Bermejo, R., 2017. Toward seashells under stress: Bioinspired concepts to design tough layered ceramic composites. J. Eur. Ceram. Soc. 37 (13), 3823–3839.
Bermejo, R., Danzer, R., 2010. Failure resistance optimisation in layered ceramics designed with strong interfaces. J. Ceram. Sci. Technol. 1, 15–20.
Borden, M.J., Hughes, T.J., Landis, C.M.., Anvari, A., Lee, I.J., 2016. A phase-field formulation for fracture in ductile materials: Finite deformation balance law derivation, plastic degradation, and stress triaxiality effects. Comput. Methods Appl. Mech. Engrg. 312, 130–166.
Bourdin, B., Francfort, G., Marigo, J.-J., 2000. Numerical experiments in revisited brittle fracture. J. Mech. Phys. Solids 48 (4), 797–826.
Bourdin, B., Francfort, G., Marigo, J.-J., 2008. The variational approach to fracture. J. Elasticity 91 (1), 5–148.

Camanho, P.P., Erçin, G.H., Catalanotti, G., Mahdi, S, Linde, P., 2012. A finite fracture mechanics model for the prediction of the open-hole strength of composite laminates. Composites A 43 (8), 1219–1225.
Carollo, V., Reinoso, J., Paggi, M., 2017. A 3D finite strain model for intralayer and interlayer crack simulation coupling the phase field approach and cohesive zone model. Compos. Struct. 182, 636–651.
Carollo, V., Reinoso, J., Paggi, M., 2018. Modeling complex crack paths in ceramic laminates: A novel variational framework combining the phase field method of fracture and the cohesive zone model. J. Eur. Ceram. Soc. 38 (8), 2994–3003.
Carpinteri, A., 1982. Notch sensitivity in fracture testing of aggregative materials. Eng. Fract. Mech. 16 (4), 467–481.
Carpinteri, A., Cornetti, P., Pugno, N., Sapora, A., Taylor, D., 2008. A finite fracture mechanics approach to structure with sharp V-notches. Eng. Fract. Mech. 75 (7), 1736–1752.
Carraro, P.A., Quaresimin, M., 2014. Modelling fibre-matrix debonding under biaxial loading. Composites A 61, 33–42.
Chao-Correas, A., Cornetti, P., Corrado, M., Sapora, A., 2022. Finite fracture mechanics extension to dynamic loading scenarios. Int. J. Fract. 1, 1–17.
Cook, T.S., Erdogan, F., 1972. Stresses in bonded materials with a crack perpendicular to the interface. Internat. J. Engrg. Sci. 10 (8), 677–697.
Cook, J., Gordon, J.E., 1964. A mechanism for the control of crack propagation in all-brittle systems. Proc. R. Soc. Lond. Ser. A Math. Phys. Eng. Sci. 282 (1391), 508–520.
Cornetti, P., Muñoz-Reja, M., Sapora, A., Carpinteri, A., 2019. Finite fracture mechanics and cohesive crack model: Weight functions vs. cohesive laws. Int. J. Solids Struct. 156–157, 126–136.
Cornetti, P., Pugno, N., Carpinteri, A., Taylor, D., 2006. Finite fracture mechanics: A coupled stress and energy failure criterion. Eng. Fract. Mech. 73 (14), 2021–2033.
Cornetti, P., Sapora, A., Carpinteri, A., 2016. Short cracks and V-notches: Finite Fracture Mechanics vs. Cohesive Crack Model. Eng. Fract. Mech. 168, 2–12.
Dugdale, D.S., 1960. Yielding of steel sheets containing slits. J. Mech. Phys. Solids 8 (2), 100–104.
Erdogan, F., Sih, G.C., 1963. On the crack extension in plates under plane loading and transverse shear. Trans. ASME D 85 (4), 519–525.
Francfort, G.A., Marigo, J.-J., 1998. Revisiting brittle fracture as an energy minimization problem. J. Mech. Phys. Solids 46 (8), 1319–1342.
García, I.G., 2014. Crack Initiation in Composites At Micro and Meso Scales: Development and Applications of Finite Fracture Mechanics (Ph.D. thesis). School of Engineering, University of Seville.
García, I.G., Carter, B.J., Ingraffea, A.R, Mantič, V., 2016. A numerical study of transverse cracking in cross-ply laminates by 3D finite fracture mechanics. Composites B 95, 475–487.
García, I.G., Leguillon, D., 2012. Mixed-mode crack initiation at a V-notch in presence of an adhesive joint. Int. J. Solids Struct. 49 (15–16), 2138–2149.
García, I.G., Paggi, M., Mantič, V., 2014. Fiber-size effects on the onset of fiber–matrix debonding under transverse tension: A comparison between cohesive zone and finite fracture mechanics models. Eng. Fract. Mech. 115, 96–110.
Griffith, A.A., 1921. The phenomena of rupture and flow in solids. Phil. Trans. R. Soc. A 221, 163–198.
Hansen-Dörr, A.C., Dammaß, F., de Borst, B., Kästner, M., 2020. Phase-field modeling of crack branching and deflection in heterogeneous media. Eng. Fract. Mech. 232, 107004.
He, M.-Y., Bartlett, A.G., Evans, A., Hutchinson, J.W., 1991. Kinking of a crack out of an interface: Role of in-plane stress. J. Am. Ceram. Soc. 74 (4), 767–771.
He, M.-Y., Hutchinson, J.W., 1989. Crack deflection at an interface between dissimilar elastic materials. Int. J. Solids Struct. 25 (9), 1053–1067.
Hussain, M., Pu, S., Underwood, J., 1973. Strain energy release rate for a crack under combined mode I and mode II. In: Proceedinmgs of the 1973 National Symposium on Fracture Mechanics, Volume 11. ASTM Special Technical Puiblications, pp. 2–28.
Hutchinson, J.W., Suo, Z., 1992. Mixed mode cracking in layered materials. Adv. Appl. Mech. 29, 63–191.
Kristensen, P.K., Martínez-Pañeda, E., 2020. Phase field fracture modelling using quasi-newton methods and a new adaptive step scheme. Theor. Appl. Fract. Mech. 107, 102446.
Kristensen, P.K., Niordson, C.F., Martínez-Pañedas, E., 2021. An assessment of phase field fracture: crack initiation and growth. Phil. Trans. R. Soc. A 379 (2203), 20210021.
Kumar, A., Bourdin, B., Francfort, G.A., Lopez-Pamies, O., 2020. Revisiting nucleation in the phase-field approach to brittle fracture. J. Mech. Phys. Solids 142, 104027.
Leblond, J.B., 1989. Crack paths in plane situations-I. General form of the expansion of the stress intensity factors. Int. J. Solids Struct. 25 (1), 1311–1325.
Leguillon, D., 2002. Strength or toughness? A criterion for crack onset at a notch. Eur. J. Mech. Solids 21 (1), 61–72.
Leite, A., Mantič, V., París, F., 2021. Crack onset in stretched open hole PMMA plates considering linear and non-linear elastic behaviours. Theor. Appl. Fract. Mech. 114, 102931.
Li, J., Leguillon, D., 2018. Finite element implementation of the coupled criterion for numerical simulations of crack initiation and propagation in brittle materials. Theor. Appl. Fract. Mech. 93, 105–115.
Lin, K.Y., Mar, J.W., 1976. Finite element analysis of stress intensity factors for cracks at a bi-material interface. Int. J. Fract. 12 (4), 521–531.
Liu, Z.-E., Wei, Y., 2021. An analytical solution to the stress fields of kinked cracks. J. Mech. Phys. Solids 156, 104619.
Maimí, P., Camanho, P.P., Mayugo, J.A., Turon, A., 2011. Matrix cracking and delamination in laminated composites. Part I: Ply constitutive law, first ply failure and onset of delamination. Mech. Mater. 43 (4), 169–185.
Mantič, V., 2009. Interface crack onset at a circular cylindrical inclusion under a remote transverse tension. Application of a coupled stress and energy criterion. Int. J. Solids Struct. 46 (6), 1287–1304.
Martínez, D., Gupta, V., 1994. Energy criterion for crack deflection at an interface between two orthotropic media. J. Mech. Phys. Solids 42 (8), 1247–1271.
Martínez-Pañeda, E., Golahmar, A., Niordson, C.F., 2018. A phase field formulation for hydrogen assisted cracking. Comput. Methods Appl. Mech. Engrg. 342, 742–761.
Miehe, C., Hofacker, M., Schänzel, L.-M., Aldakheel, F., 2015. Phase field modeling of fracture in multi-physics problems. Part II. Coupled brittle-to-ductile failure criteria and crack propagation in thermo-elastic–plastic solids. Comput. Methods Appl. Mech. Engrg. 294, 486–522.
Miehe, C., Hofacker, M., Welschinger, F., 2010. A phase field model for rate-independent crack propagation: Robust algorithmic implementation based on operator splits. Comput. Methods Appl. Mech. Engrg. 199 (45), 2765–2778.
Molnár, G., Doitrand, A., Estevez, R., Gravouil, A., 2020. Toughness or strength? Regularization in phase-field fracture explained by the coupled criterion. Theor. Appl. Fract. Mech. 109, 102736.
Muñoz-Reja, M., Távara, L., Mantič, V., Cornetti, P., 2020. A numerical implementation of the Coupled Criterion of Finite Fracture Mechanics for elastic interfaces. Theor. Appl. Fract. Mech. 108, 102607.
Nguyen, T.T., Yvonnet, J., Bornert, M., Chateau, C., Sab, K., Romani, R., Le Roy, R., 2016a. On the choice of parameters in the phase field method for simulating crack initiation with experimental validation. Intern. J. Fract. 197, 213–226.
Nguyen, T.T., Yvonnet, J., Zhu, Q.-Z., Bornert, M., Chateau, C., 2016b. A phase-field method for computational modeling of interfacial damage interacting with crack propagation in realistic microstructures obtained by microtomography. Comput. Methods Appl. Mech. Engrg. 312, 567–595, Phase Field Approaches to Fracture.
Paggi, M., Reinoso, J., 2017. Revisiting the problem of a crack impinging on an interface: a modeling framework for the interaction between the phase field approach for brittle fracture and the interface cohesive zone model. Comput. Methods Appl. Mech. Engrg. 321, 145–172.
Parmigiani, J.P., Thouless, M.D., 2006. The roles of toughness and cohesive strength on crack deflection at interfaces. J. Mech. Phys. Solids 54 (2), 266–287.

Quintanas-Corominas, A., Turon, A., Reinoso, J., Casoni, E., Paggi, M., Mayugo, J.A, 2020. A phase field approach enhanced with a cohesive zone model for modeling delamination induced by matrix cracking. Comput. Methods Appl. Mech. Engrg. 358, 112618.
Reinoso, J., Paggi, M., 2014. A consistent interface element formulation for geometrical and material nonlinearities. Comput. Mech. 54 (6), 1569–1581.
Rosendahl, P.L., Staudt, Y., Schneider, A.P., Schneider, J., Becker, W., 2019. Nonlinear elastic finite fracture mechanics: Modeling mixed-mode crack nucleation in structural glazing silicone sealants. Mater. Des. 182, 108057.
Roy Xu, L., Huang, Y., Rosakis, A., 2003. Dynamic crack deflection and penetration at interfaces in homogeneous materials: Experimental studies and model predictions. J. Mech. Phys. Solids 51 (3), 461–486.
Schellekens, J., Borst, R.D., 1993. On the numerical integration of interface elements. Internat. J. Numer. Methods Engrg. 36 (1), 43–66.
Stein, N., Dölling, S., Chalkiadaki, K., Becker, W., Weissgraeber, P., 2017. Enhanced XFEM for crack deflection in multi-material joints. Int. J. Fract. 207, 193–210.
Sundaram, B.M., Tippur, H., 2016. Dynamics of crack penetration vs. branching at a weak interface: An experimental study. J. Mech. Phys. Solids 96, 312–332.
Tada, H., Paris, P., Irwin, G., 2000. The Stress Analysis of Cracks Handbook. John Wiley & Sons, London.
Takeda, N., Ogihara, S., 1994. In situ observation and probabilistic prediction of microscopic failure processes in CFRP cross-ply laminates. Compos. Sci. Technol. 52 (2), 183–195.
Tanné, E., Li, T., Bourdin, B., Marigo, J.-J., Maurini, C., 2018. Crack nucleation in variational phase-field models of brittle fracture. J. Mech. Phys. Solids 110, 80–99.
Teichtmeister, S., Kienle, D., Aldakheel, F., Keip, M.-A., 2017. Phase field modeling of fracture in anisotropic brittle solids. Int. J. Non-Linear Mech. 97, 1–21.
Tullock, D.L., Reimanis, I.E., Graham, A.L., Petrovic, J.J., 1994. Deflection and penetration of cracks at an interface between two dissimilar materials. Acta Metall. Mater. 42 (9), 3245–3252.
Turon, A., Camanho, P.P., Costa, J., Dávila, C.G., 2006. A damage model for the simulation of delamination in advanced composites under variable-mode loading. Mech. Mater. 38 (11), 1072–1089.
Wang, X., Wang, C., Atkinson, A., 2012. Interface fracture toughness in thermal barrier coatings by cross-sectional indentation. Acta Mater. 60, 6152–6163.
Weißgraeber, P., Leguillon, D., Becker, W., 2016. A review of Finite Fracture Mechanics: crack initiation at singular and non-singular stress raisers. Arch. Appl. Mech. 86 (1), 375–401.
Wu, J.-Y., Huang, Y., 2020. Comprehensive implementations of phase-field damage models in Abaqus. Theor. Appl. Fract. Mech. 106, 102440.
Wu, J.-Y., Nguyen, V.P., 2018. A length scale insensitive phase-field damage model for brittle fracture. J. Mech. Phys. Solids 119, 20–42.
Yosibash, Z., Priel, E., Leguillon, D., 2006. A failure criterion for brittle elastic materials under mixed mode loading. Int. J. Fract. 141 (1), 289–310.
Zambrano, J., Toro, S., Sánchez, P.J., Duda, F.P, Méndez, C.G., Huespe, A.E., 2022. Interaction analysis between a propagating crack and an interface: Phase field and cohesive surface models. Int. J. Plast. 156, 103341.
Zeng, X., Wei, Y., 2017. Crack deflection in brittle media with heterogeneous interfaces and its application in shale fracking. J. Mech. Phys. Solids 101, 235–249.
Zhang, Z., Suo, Z., 2007. Split singularities and the competition between crack penetration and debond at a bimaterial interface. Int. J. Solids Struct. 44 (13), 4559–4573.
Zubillaga, L., Turon, A., Maimí, P., Costa, J., Mahdi, S., Linde, P., 2014. An energy based failure criterion for matrix crack induced delamination in laminated composite structures. Compos. Struct. 112, 339–344.